**Original Research Article**

# QSAR modelling of novel coumarin derivatives for MAO-B inhibition


## Abstract

We report here the design of new inhibitors against human monoamine oxidase (*h*MAO-B) as potential treatment of Parkinson's disease. We have completed computer-aided molecular design of MAO-B inhibitors by *in situ* modification of the reference crystal structure of *7-(3-chlorobenzyloxy)-4-(methylamino) methyl-coumarin cocrystallized*(COU1) in complex with MAO-B (Protein Data Bank (PDB) entry code: 2v61) using MM-PB approach. A QSAR model built for a training set of 29 COUs with reported inhibitory activities ($IC_{50}^{exp}$) displayed a significant correlation between the computed relative Gibbs free energies (rGFE, $\Delta\Delta G_{com}$) of MAO-B – inhibitor complex formation and $IC_{50}^{exp}$ ($pIC_{50}^{exp}$ = -0.22.$\Delta\Delta G_{com}$ +7.73; $R^2$ = 0.93). With this QSAR model we were able to explain almost 93% of the variation of observed inhibition data. The predictive capability of the QSAR model was validate by generating the 3D QSAR MAO-B inhibition Pharmacophore (PH4) the estimated $IC_{50}^{pred}$ of which displayed a non-less significant correlation with the observed $IC_{50}^{exp}$($R^2$ = 0.91) making this PH4 a reliable chemical space virtual screening tool.Deep analysis of MAO-B – inhibitor interactions at the enzyme active site suggested structural information about interesting building blocks for enumerating a large and diverse virtual combinatorial library (VCL) of 67,949 analogues of the reference inhibitor (COU1). The best PH4 mapping hit emerging from the virtual screening displays a half-maximal inhibitory concentration of 20 pM.Combining molecular modeling and PH4 model resulted in proposed novel potent anti-Parkinson's agent candidates with favorable pharmacokinetic profiles.Despite the lack of Molecular Dynamics (MD) check of the conformational stability of novel predicted potent analogues, the resulting PH4, as virtual screening tool,can help processing larger databases in search of coumarin scaffold bearing MAO-B inhibitors.



KEYWORDS

Coumarin inhibitors; human monoamine oxidase B (*h*MAO-B); coumarins derivatives (COUs); quantitative structure-activity relationships (QSAR); pharmacophore (PH4); molecular modeling.


## 1. INTRODUCTION

"Monoamine oxidase (MAO, EC.1.4.3.4, amine-oxygen oxidoreductase) is a membrane-bound flavoenzyme responsible for the oxidative deamination of xenobiotic amines" [1] and monoamine neurotransmitters such as serotonin (5-HT), norepinephrine (NE), and dopamine (DA)[2]. "The enzyme exists in two forms, *h*MAO-A and *h*MAO-B, encoded by different genes and differing in tissue distribution, structure and substrate specificity" [3]. "By inhibiting *h*MAO, the degradation of monoamines is blocked, leading to an increase in their availability for their physiological fonctions. In keeping with these premises, the development of *h*MAO inhibitors has led to important break-throughs in the therapy of several neuropsychiatric disorders" [4].

"In recent years, interest in selective *h*MAO-B inhibitors has increased significantly due to the discovery that expression levels of this isoenzyme in neuronal tissue increase 4-fold with age, resulting in an increment of dopamine metabolism, as well as of production of hydrogen peroxide, causative of oxidase stress and may play a relevant role in the etiology of neurodegenerative diseases" [5]. "As a result, MAO-B inhibitors woulduseful as adjuvant for the treatment of Parkinson's disease. Crystal structures revealed that residues Ile199" [6,7] and Tyr326 [8] specifically and catalytically, are important for ligandbinding. "The aromatic cagedelimited by Tyr398 and Tyr435 plays a key role in coordinating ligands in the active site to the FAD molecule [9]. Several different MAO-B inhibitors are used against Parkinson's disease, including" [10]:selegiline hydrochloride(tablets,orally disintegrating tablet), rasagiline(tablet) and safinamide(tablet).

"The irreversible inhibitors of MAO-B, selegiline and rasagiline, are used clinically in treatment of Parkinson's disease, and a recently introduced reversible MAO-B inhibitor, safinamide, has also been shown to be effective. Modification of the pharmacokineticcharacteristics of these inhibitors has led to development of new drug formagainst Parkinson's disease.

In this study we focused on validating the binding modes of a series of 33 coumarin derivatives (COU) with reported experimental MAO-B inhibitory activity in the nanomolar range"[11], the most active of which is the endogenous ligand of the deposited RX crystallography structure in complex with MAO-B (PDB code 2V61). From a training set (TS) of 29 coumarin derivatives (COU1-29) and a validation set of 4 COU30-33, aone descriptor QSAR model of MAO-B inhibition was built by *in situ* modification of the reference inhibitor COU1 in the above mentioned3D structure 2v61.pdb in the gas phase and in the solvent taking account of biological medium solvation. This model correlates the relative Gibbs free energy (rGFE) of MAO-B – COU1-30 complex formation with observed ($IC_{50}^{exp}$). A 3D pharmacophore (PH4)was generated from the QSAR identified active conformation of COUs in order to screen the coumarins COUs chemical subspace for novel COUs analogues with predicted better potency and favorable pharmacokinetic profile.

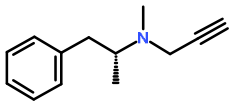

**Pic2 : Selegiline ($IC_{50}$ = 6.8 nM, [12])**

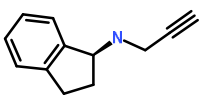

**Pic3 : Rasagiline ($IC_{50}$ = 14 nM)**

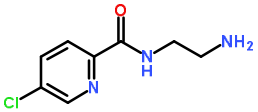

**Pic 4 :Lazabemide**

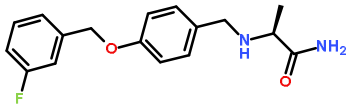

**Pic 5 :Safinamide**

**($IC_{50}$ = 30nM [13])** **($K_i$ = 0,45 µM, [14])**

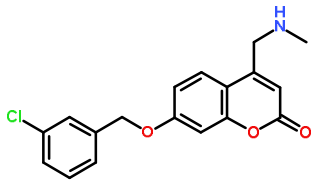

**Pic1: 7-[(3-chorobenzyl)oxy]-4-[(methylamino)-methyl]-2H-chromen-2-one methanesulfonate (COU1, $IC_{50}^{exp}$ = 13 nM,[11])**

## 2. MATERIALS AND METHODS

### 2.1. Training sets

Structural studies and bioassays ($IC_{50}^{exp}$) of our studied coumarin derivatives (COU) MAO-B inhibitors were retrieved fromP. Leonardo *et al.*[11]. The efficacy range of inhibitory concentrations (13≤ $IC_{50}^{exp}$ ≤ 16,100 nM), allows us to realize QSAR models. The whole series of 33 COUs were divided into a training (TS) and a validation (VS) setsof 29 and 4 COUs respectively. [11].

### 2.2. Model building

The entire complex (E:I), with free MAO-B (E) and inhibitor (I) was resolved to a reliability factor of 1.7 Å containing the 7-[(3-chorobenzyl)oxy]-4-[(methylamino)-methyl]-2H-chromen-2-onemethanesulfonate (COU1) bound to MAO-B (Whose crystallographic data entrycode 2v61[15])from Discovery Studio 2.5 software. [16].Virtual design plan to result in new COU analogues with higher predicted activity is presented in scheme1. The structures (E and E : I complexes) were at the neutral pH=7 and neutral N- and C-terminal residues, all protonizable and ionizable aminoacidsbeing charged, without any crystallographic water molecules. The inhibitors were built into the 2v61structure by *in situ* replacing derivativegroups of the COU1 moiety followed by systematic conformational search of the replacing group coupled with a careful energy-minimizationof the modifiedinhibitor and surrounding MAO-B active site residues[17, 18, 19, 20, 21, 22, 23, 24, 25, 26, 27, 28, 29, 30, 31, 32].

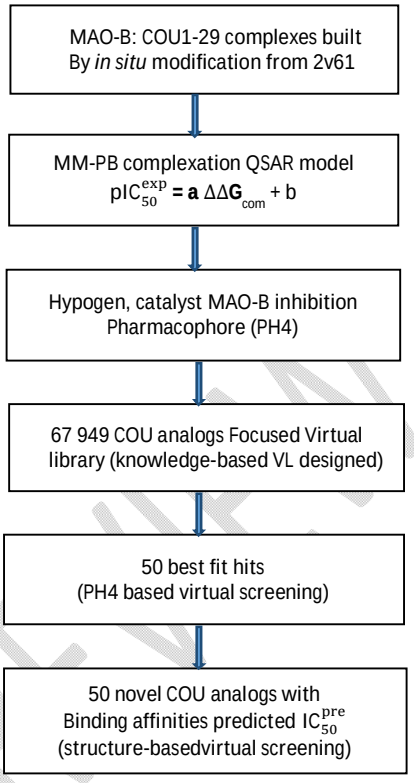


Scheme 1.Virtual design plan to result in new COU analogues with higher predicted

### 2.3.MOLECULAR MECHANICS

Molecular mechanics, a fundamental method of our work has been previously described by[21,30]

### 2.4.Conformational search

For conformational research we recommend reading the following articles [16, **Error! Bookmark not defined.**, **Error! Bookmark not defined.**].

### 2.5. Solvation Gibbs free energies

As for the free solvation energy has been describedperfectly by the following articles [**Error! Bookmark not defined.**,**Error! Bookmark not defined.**,30].

### 2.6. CALCULATION OF BINDING AFFINITY AND QSAR MODEL

The methods for exploring the QSAR and the binding affinity have been described by the articles whose references are[15,16,33].

Inhibition constant ($K_i$) of a reversible inhibitor I is related to the standard Gibbs free energy (GFE) change upon formation of the enzyme-inhibitor (E:I) complexes ($\Delta G_{comp}$) in a solvent. Thus prediction of $K_i$ value from the complexation GFE as $\ln K_i = \Delta G_{comp}/RT$, is achievable assuming the following equilibrium: $\{E\}_{aq} + \{I\}_{aq} \leftrightarrow \{E:I\}_{aq}$ (1)

where $\{\ \}_{aq}$indicates solvated species. Half-maximal inhibitory concentration $IC_{50}$ is for tight binding competitive inhibitors proportional to $K_i$:

$IC_{50} = K_i (S/K_m +1) +E/2$

where S is the substrate concentration, $K_m$ represents the Michaelis constant and E means the free enzyme concentration [34]. The standard GFE change of the reaction (1) can be derived by molecular simulations of the complex and the free reactants:

$\Delta G_{comp} = G\{E:I\}- G\{E\}-G\{I\}$ (2)

In this work we approximate the exact values of standard GFE for larger systems such as enzyme-inhibitor complexes by the expression [**Error! Bookmark not defined.**, **Error! Bookmark not defined.**]: $G\{E:I\}\approx E_{MM}\{E:I\}+RT-TS_{trv}\{E:I\}+G_{solv}\{E:I\}$ (3)

Where $E_{MM}$ {E:I} stands for the MM total energy of the complex (including bonding and non-bonding contributions), $G_{solv}${E:I} is the solvation GFE contribution, and $TS_{trv}${E:I} is the entropic term :

$TS_{trv}\{E:I\}=TS_{tran}\{E:I\} + TS_{rot}\{E:I\} + TS_{vib}\{E:I\}$ (4)

Composed of the sum of contribution arising from translational, rotational and vibrational motions of E:I. Assuming that the tran and rot terms for the complex E:I and free enzyme E are approximately equal, we obtain:

$\Delta G_{comp}\approx[E_{MM}\{E:I\}-E_{MM}\{E\}-E_{MM}\{I\}]+[G_{solv}\{E:I\}-G_{solv}\{E\}-G_{solv}\{I\}]+TS_{tran}\{I\}+TS_{rot}\{I\}-[TS_{vib}\{E:I\}-TS_{vib}\{E\}-TS_{vib}\{I\}]=\Delta H_{MM}+TS_{tran}\{I\}+TS_{rot}\{I\}-\Delta TS_{vib}+\Delta G_{solv}$ (5)

Where $TS_{tran}${I} and $TS_{rot}${I} describe the translational and rotational entropy term of the free inhibitor and $\Delta TS_{vib}$ represents a simplified vibrational entropy change upon the complex formation.

Comparison between different inhibitors was done via relative changes in the complexation GFE with respect to a reference inhibitor, $I_{ref}$, assuming ideal gas behaviour for the rotational and translational motions of the inhibitors:

$\Delta\Delta G_{comp}=\Delta G_{comp}(I)-\Delta G_{comp}(I_{ref})=\Delta\Delta H_{MM} - \Delta\Delta TS_{vib}+\Delta\Delta G_{solv}$(6)

The evaluation of relative changes is preferable as it is expected to lead to partial cancellation of errors caused by the approximate nature of the molecular mechanics method as well as solvent and entropic effects description. Quantitative structure-activity relationships (QSAR), in which a linear relationship between the computed relative Gibbs free energies of the MAOB-COU complex formation $\Delta\Delta G_{com}$ for the receptor and observed inhibitory potencies $IC_{50}^{exp}$ specific to Parkinson disease, assumed according to Equations (1) and (2):

$pIC_{50}^{exp} = -\log_{10} IC_{50}^{exp} = a.\Delta\Delta G_{com} + b$ (7)

The QSAR model was prepared by linear regression for the training set of COUs[11] using $\Delta\Delta G_{com}$ quantities calculated from Equation (6), where a and b are regression coefficients. This QSAR model (termed here also as a target-specific scoring function) was then evaluated with help of validation set, not included into the training set, and employed for prediction of inhibitory potencies ($IC_{50}^{exp}$) of newly designed and modeled COU analogues.

### 2.7. Interaction energy

For interaction energy refer to the full description we reported formerly[16,**Error! Bookmark not defined.**, **Error! Bookmark not defined.**].

### 2.8. Pharmacophore generation

The pharmacophore generation from active conformation of COU1-29 from the 3D QSAR pharmacophore protocol by catalyst HypoGen algorithm [35] implemented in Discovery Studio [16] has been fully described formerly [30].

## 3-RESULTS

We selected 29 COUs as a training set and 4 COUs as a validation set (Table 1) designed from the same laboratory with their given inhibitory activity. [11]. All of our compounds were generated by substitutions on the R1 and R2 groups of the coumarin derivative scaffold, as shown in Table 1. Their experimental inhibitory activity $IC_{50}^{exp}$ has a significant gap to build a reliable model of COU inhibitor.

**Table 1**Composition of the COUs series, training set and validation set[11]are used to base the QSAR of inhibitors binding. Substituants R1 and R2 are numbered in the table as group index #R≡.group index.

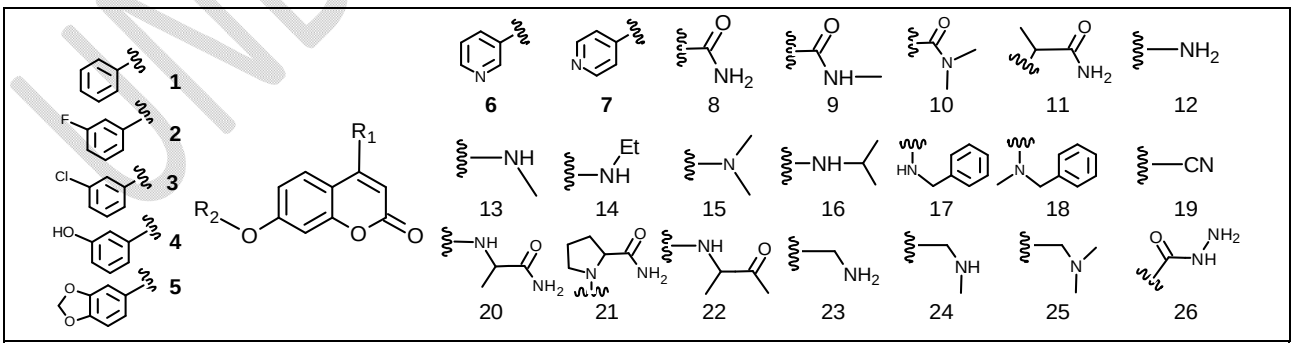


| Training set | COU1 | COU2 | COU3 | COU4 | COU5 | COU6 | COU7 | COU8 | COU9 | COU10 | COU11 | COU12 |
|---|---|---|---|---|---|---|---|---|---|---|---|---|
| $\#R_1–\#R_2$ | 13–3 | 9–1 | 13–2 | 13–5 | 12–1 | 9–3 | 13–1 | 8–3 | 26–1 | 10–3 | 8–2 | 26–3 |
| $K_i$ (nM) | 13 | 15 | 18 | 20 | 21 | 24 | 28 | 30 | 40 | 40 | 50 | 90 |

| Training set | COU13 | COU14 | COU15 | COU16 | COU17 | COU18 | COU19 | COU20 | COU21 | COU22 | COU23 | COU24 |
|---|---|---|---|---|---|---|---|---|---|---|---|---|
| $\#R_1-\#R_2$ | 14–2 | 11–1 | 11–2 | 8–1 | 20–3 | 19–1 | 23–3 | 24–3 | 15–2 | 15–3 | 6–1 | 20–1 |
| $K_i$ (nM) | 100 | 100 | 100 | 200 | 210 | 230 | 250 | 300 | 510 | 1120 | 1300 | 1800 |

| Training set | COU25 | COU26 | COU27 | COU28 | COU29 | Validation set | COU30 | COU31 | COU32 | COU33 |
|---|---|---|---|---|---|---|---|---|---|---|
| $\#R_1-\#R_2$ | 7–1 | 17–3 | 18–3 | 21–3 | 21–1 | $\#R_1-\#R_2$ | 16–2 | 25–1 | 8–4 | 10–1 |
| $K_i$ (nM) | 2000 | 3600 | 8000 | 9600 | 16100 | $K_i$ (nM) | 3800 | 460 | 1000 | 400 |

### 3.1. Quantitative Structure-Activity Relationships model

The GFE of the MAOB-COU1 complex was used to build the QSAR model. See (Fig. 1) in the site we carried out end-to-end modification of the R1 and R2 fragments if possible to achieve compounds from the test set and the validation set. The link to our database is as follows: (PDB entry code 2v61 [15]). Table 2 provides us with information on the molecular masses, the enthalpy in the gaseous medium, the enthalpy in the solvated medium with their inhibitory activity respectively of our compounds of coumarins derivatives inhibitors [11].

Our model establishes a link between inhibitory activity and the $\Delta\Delta G_{com}$ [11]. First the exploratory model in gas phase $pIC_{50}^{exp}$ =f ($\Delta\Delta H_{MM}$) and the deepest insight model (solvation and inhibitor vibrational entropy loss)$pIC_{50}^{exp}$ =f ($\Delta\Delta G_{com}$) all in Table 3 and Figure 2. Statistical data such as determination coefficient and Fischer F-test suggest strong connection between the binding model and $pIC_{50}^{exp}$of COUs.

**Table 2**. Complexation Gibbs free energy (binding affinity) and its components for the training set (TS) of MAO-B inhibitors COU1-29 and validation set (VS) inhibitors COU30-33.

| Training set[a] | $M_w$[b] | $\Delta\Delta H_{MM}$[c] | $\Delta\Delta G_{sol}$[d] | $\Delta\Delta TS_{vib}$[e] | $\Delta\Delta G_{com}$[f] | $IC_{50}^{exp}$[g] |
|---|---|---|---|---|---|---|
| COU1 | 329 | 0 | 0 | 0 | 0 | 13 |
| COU2 | 323 | 0.07 | 1.91 | 1.95 | 0.03 | 15 |
| COU3 | 313 | 0.78 | 0.38 | 0.43 | 0.74 | 18 |
| COU4 | 339 | 0.93 | -1.23 | -1.14 | 0.84 | 20 |
| COU5 | 281 | 1.32 | -0.63 | 0.73 | -0.04 | 21 |
| COU6 | 357 | -0.91 | 2.27 | 0.10 | 1.25 | 24 |
| COU7 | 295 | 2.81 | 0.87 | 2.41 | 1.27 | 28 |
| COU8 | 343 | 0.12 | 1.25 | -1.79 | 3.17 | 30 |
| COU9 | 324 | 2.03 | 0.40 | 2.07 | 0.35 | 40 |
| COU10 | 371 | -0.13 | 0.27 | -2.83 | 2.98 | 40 |
| COU11 | 327 | 1.38 | 0.54 | -1.44 | 3.36 | 50 |
| COU12 | 358 | 0.95 | 0.67 | 0.20 | 1.41 | 90 |
| COU13 | 327 | 1.51 | 1.50 | 0.50 | 2.51 | 100 |
| COU14 | 323 | 2.48 | 1.17 | 0.98 | 2.68 | 100 |
| COU15 | 341 | 1.42 | 1.06 | 0.06 | 2.43 | 100 |
| COU16 | 309 | 2.95 | 0.33 | -0.24 | 3.52 | 200 |
| COU17 | 372 | 0.70 | 1.65 | -2.46 | 4.81 | 210 |
| COU18 | 291 | 4.15 | 0.41 | -0.12 | 4.69 | 230 |
| COU19 | 329 | 0.66 | 2.37 | -0.33 | 3.25 | 250 |
| COU20 | 343 | 3.10 | 2.71 | -0.20 | 6.01 | 300 |
| COU21 | 327 | 2.00 | 1.29 | -1.08 | 4.36 | 510 |
| COU22 | 343 | 6.40 | 2.09 | -0.72 | 9.22 | 1120 |
| COU23 | 310 | 4.50 | 0.73 | -3.10 | 8.33 | 1300 |
| COU24 | 352 | 6.28 | 3.58 | 2.57 | 7.29 | 1800 |
| COU25 | 310 | 4.94 | 2.55 | -2.51 | 10.01 | 2000 |
| COU26 | 405 | 6.71 | 3.70 | -1.56 | 11.97 | 3600 |
| COU27 | 419 | 9.49 | 0.45 | -1.28 | 11.22 | 8000 |
| COU28 | 398 | 6.69 | 5.88 | 0.47 | 12.09 | 9600 |
| COU29 | 364 | 8.82 | 5.87 | 2.18 | 12.51 | 16100 |

| Validation set | $M_w$[b] | $\Delta\Delta H_{MM}$[c] | $\Delta\Delta G_{sol}$[d] | $\Delta\Delta TS_{vib}$[e] | $\Delta\Delta G_{com}$[f] | $\frac{pIC_{50}^{pre}}{pIC_{50}^{exp}}$ |
|---|---|---|---|---|---|---|
| COU30 | 341 | 9.14 | 1.53 | 0.91 | 9.76 | 1.029 |
| COU31 | 323 | 5.29 | 1.13 | 1.44 | 4.97 | 1.046 |
| COU32 | 325 | 3.41 | 1.69 | -1.35 | 6.45 | 1.051 |
| COU33 | 337 | 3.58 | 0.33 | -1.16 | 5.07 | 1.032 |

[a] for the chemical structures of the training set of inhibitors see Table 1; [b] $M_w$(g/mol) is the molecular mass of inhibitors ; [c] $\Delta\Delta H_{MM}$(kcal/mol) is the relative enthalpic contribution to the Gibbs free energy change related to enzyme-inhibitor (E:I) complex formation derived by molecular mechanics (MM): $\Delta\Delta H_{MM} \cong [E_{MM}\{E{:}I_x\} - E_{MM}\{I_x\}] - [E_{MM}\{E{:}I_{ref}\} - E_{MM}\{I_{ref}\}]$, $I_{ref}$ is the reference inhibitor COU1; [d] $\Delta\Delta G_{sol}$(kcal/mol) is the relative solvation Gibbs free energy contribution to the Gibbs free energy change of E:I complex formation: $\Delta\Delta G_{sol} = [G_{sol}\{E{:}I_x\} - G_{sol}\{I_x\}] - [G_{sol}\{E{:}I_{ref}\} - G_{sol}\{I_{ref}\}]$; [e] $\Delta\Delta TS_{vib}$(kcal/mol) isthe relative entropic contribution of inhibitor $I_x$ to the Gibbs free energy related to E:I complex formation: $\Delta\Delta TS_{vib} = [\Delta\Delta TS_{vib}\{I_x\}_E - \Delta\Delta TS_{vib}\{I_x\}] - [\Delta\Delta TS_{vib}\{I_{ref}\}_E - \Delta\Delta TS_{vib}\{I_{ref}\}]$; [f] $\Delta\Delta G_{com} \cong \Delta\Delta H_{MM} + \Delta\Delta G_{sol} - \Delta\Delta TS_{vib}$(kcal/mol) is the relative Gibbs free energy change related to E:$I_x$ complex formation; [g] $IC_{50}^{exp}$ is the experimental half-maximal inhibitory concentration (in nM) obtained from reference[11]; [h] Ratio of predicted and experimental half-maximal inhibition concentrations $pIC_{50}^{pre}/pIC_{50}^{exp}$ ($pIC_{50}^{pre} = -\log_{10}IC_{50}^{pre}$) was predicted from computed $\Delta\Delta G_{com}$ using the regression equation shown in Table 3.

**Table 3**. Regression analysis of computed binding affinities $\Delta\Delta G_{com}$, its enthalpic component $\Delta\Delta H_{MM}$, and experimental $IC_{50}^{exp}$ of coumarin derivatives (COUs) towards MAO-B:$pIC_{50}^{exp} = -\log_{10}(IC_{50}^{exp})$.

| Statistical Data of Linear Regression | (A) | (B) |
|---|---|---|
| **$pIC_{50} = -0.30 \times \Delta\Delta H_{MM} + 7.55$ (A)** | | |
| **$pIC_{50} = -0.22 \times \Delta\Delta G_{com} + 7.73$ (B)** | | |
| Number of compound n | 29 | 29 |
| Square correlation coefficient of regression $R^2$ | 0.82 | 0.93 |
| LOO cross-validated square correlation coefficient $R^2_{xv}$ | 0.81 | 0.93 |
| Standard error of regression $\sigma$ | 0.40 | 0.24 |
| Statistical significance of regression, Fisher F-test | 120.5 | 375.1 |
| Level of statistical significance $\alpha$ (%) | >95 | >95 |
| Range of activities $IC_{50}^{exp}$ ($n$M) | 13 – 16100 | |

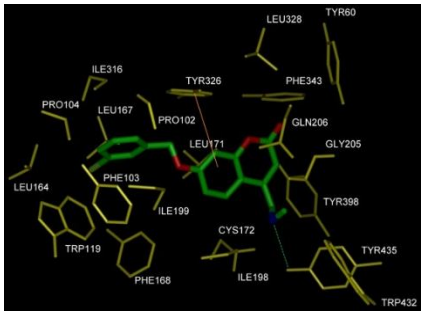

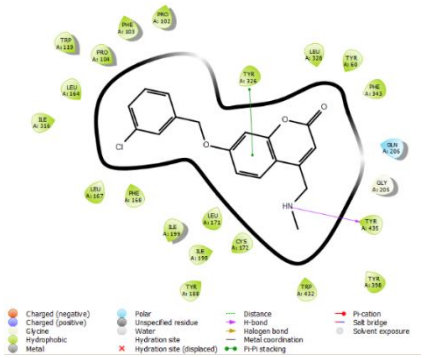

**Figure 1.** (Top) 3D schematic interaction diagram of the most potent inhibitor COU1 (Table 1) at the active-site of MAO-B protein; (Bottom) 2D structure of the active-site with bound inhibitor COU1.

The ratio $pIC_{50}^{pre}/pIC_{50}^{exp}$, with the $pIC_{50}^{pre}$computedwith Equation (**B**), Table 3 for VS COU30-33not in the TS, is near one attestingsignificant predictive capacity of the complexation QSAR model, Table 1 and 2.

### 3.2. Binding mode of inhibitors

In the crystal structure of MAO-B –COU1 [11]the substitution at R1-and R2-groups of the coumarin derivative scaffold of the inhibitor sits in a hydrophobic cavity of the active-site surrounded by side chains of predominantly nonpolar residues : Trp119, Leu164, Leu167, Phe168, Ile198, Ile199, Ile316 and Tyr326. While the R2-group at position 7 has preferred binding conformation in the hydrophobic cavity, at position 4 (R1) faces a steric hindrance giving the better affinity to smaller substituent confirmed by our QSAR model. All interactions observed in the crystal structure were conserved. As displayed in Fig. 1, the binding mode of COUs at MAO-B active site of the best active COU1 in 2D is supported by the following interactions: π-π stacking with Tyr326, hydrogen bond with Tyr435 and hydrophobic contacts. The MAO-B active site consists of two cavities, the substrate cavity in front of the flavin and the entrance cavity located underneath the protein surface [36,37].Beside the robustness of the QSAR model, the analysis of the interactions between COUs and MAO-B is expected to reveal key interactions behindE-I affinity able to guide the selection of novel potency improving substituents through more intensive hydrogen bonds (HBs), Van der Waals (VdW), hydrophobic contacts.

We analyzed contributions of individual residues of the enzyme binding pocket to the total computed enzyme-inhibitor interaction energy ($E_{int}$). In the hydrophobic pochet we have noticed a significant contribution to the $E_{int}$ from residues Trp119, Leu164, Leu167 Phe168, Ile198, Ile199, Ile316 and Tyr326. (Fig. 3).

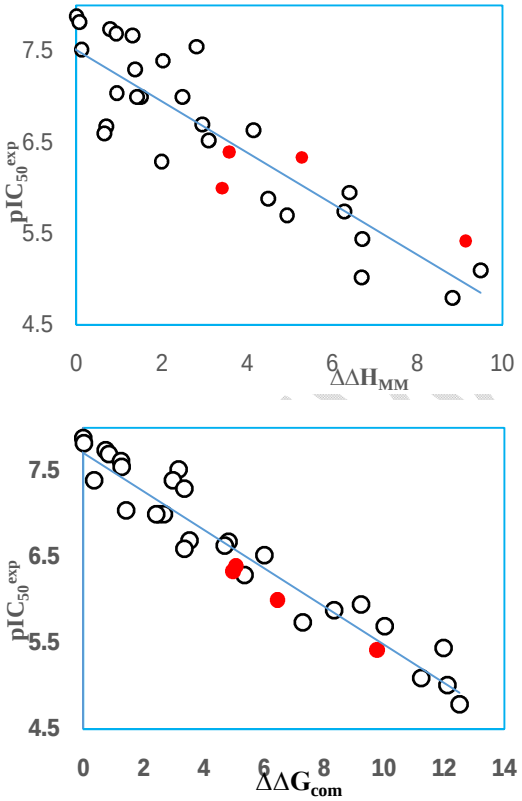


**Figure 2.** (Top)the equality curve of $pIC_{50}$ andand the enthalpy of the coumarin series in the gaseous medium ($\Delta\Delta H_{MM}$)of MAOB-COUx complex formation.; (Below) similar plot for relative complexation Gibbs free energies of the MAOB-COUx complex formation $\Delta\Delta G_{com}$of training set, all in kcal.mol$^{-1}$. Data from the validation set is shown in red; the black circles represent the COUs of the test sets.

### 3.3. Interaction Energy

in addition to the correlation curve, other structural information is obtained from the interaction energy diagram (IE, $\Delta E_{int}$) obtained for each inhibitor in the test set. Analysis of the interaction energy is an important contribution to detecting the inhibitory power of each fragment with the residues at the active site.To carry out our comparative study of interaction energy diagrams, we decided to divide our series of COUs from the test game into three parts. See fig. 3 (compounds with higher inhibitory activities, those with medium activities and those with low activities). This comparison led us to identify residues that strongly contribute to the increase of the inhibitory power of each compound. Therefore, no suggestions for suitable substitutions able to improve the binding affinity emerge suggesting a combinatorial approach where novel COU analogs virtual library is enumerated from new R-group substituents and in silico screened with help of the PH4 pharmacophore of MAO-B inhibition derived from our complexation QSAR model. A reported alternative approach through steered Molecular Dynamics Stimulations has been reported revealing in a bilayer environment per-residue interaction energy for unfortunately reduced number of MAO-B inhibitors probably due to huge time consuming computations engagedjust confirmed the key role of Tyr326,

Leu169, Gln206, Tyr398, Asp318, already noticed from crystal structure[38].

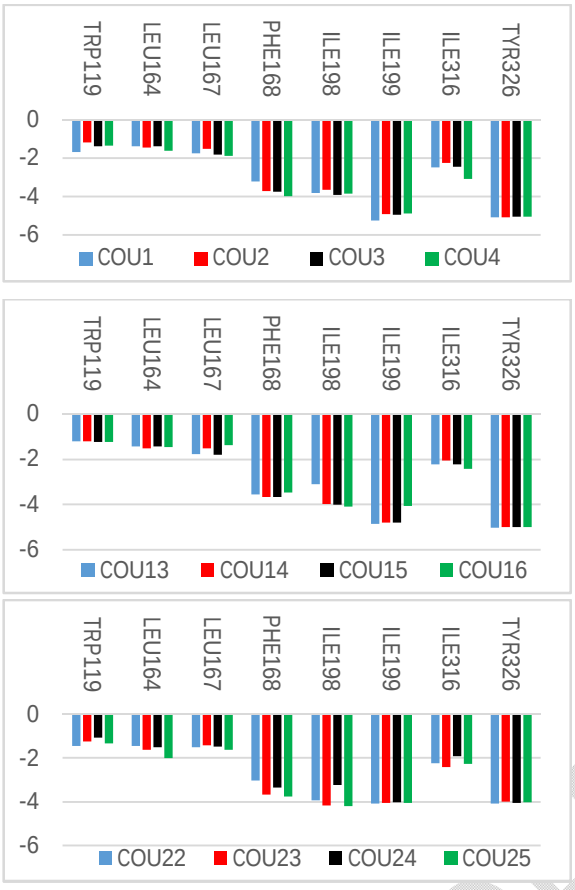


Figure 3. Mechanics intermolecular interaction energy $E_{int}$ breakdown to residue contributions in the hydrophobic pochet [kcal.mol$^{-1}$]: (Top) two most active inhibitors COU1-2, (Middle) moderately active inhibitors COU14-15, (Bottom) less active inhibitors COU23-24. Table 2 [11].

### 3.4. Pharmacophore model of inhibitory activity

The 3D-QSAR PH4 pharmacophore generation process fully has been described previously [30]. The most active TS COU1 ($IC_{50}^{exp}$ = 13$n$M and $IC_{50}^{exp}$ ≤ 2 x 13$n$M) alone served for features building and retained. The 10 optimized hypotheses with the lowest costs, 130.5 (Hypo1) to 176.4 (Hypo10)are the bests PH4 for $IC_{50}$ prediction, higher than the fixed cost (89.9), lower than the null one (260.8) both separated by a gap Δ = 170.9, very >> 70 and synonymous of high predictability. The computational process for each hypothesis namely statistical significance, Fisher randomization, CatScrambleprogrammewere describedearlier [30] and for S=98% the 10 lowest cost hypotheses built from COUs active conformation are listed in Table 4. Hypo 1 with the lowest cost (130.5),RMSD (1.575), highest $R^2$ (0.89) was retained as MAO-B inhibition PH4. The statistical data of hypotheses (costs, RMSD, $R^2$) and of the correlation plot $pIC_{50}^{exp}$ vs $pIC_{50}^{pred}$in Figure 4 ($pIC_{50}^{exp}$ = 0.75.$pIC_{50}^{pre}$ + 1.66;n =29, $R^2$ =0.91, $R_{xv}^2$ =0.90, F-test = 288.3, $\sigma$ =0.276, $\alpha$> 95%, 1.575 ≤ RMSD ≤ 2.442, 0.72 ≤ $R^2$ ≤ 0.89) document a PH4 predictive power as robust as the MM-PB complexation QSAR model with $\Delta\Delta G_{com}$ as single descriptor.To validate the PH4 model, the ratio$pIC_{50}^{pre}$ / $pIC_{50}^{exp}$for the validation set(VS, Table 1) of COU30: 1.126, COU31: 1.06, COU32: 0.998, COU33: 1.180 has been computed and the closeness toone attests its predictability.The geometry of the Hypo1 pharmacophore of MAO-B inhibition is displayed on Figure 4 with the appropriate features and their spatial coordinates. The configuration cost (9.4) << 17 the upper limit [39] also attests the PH4 quality. The use of the PH4 for virtual screening mostly is based on the inclusion of the hydrophobic feature (HYD, Figure 4) in the best PH4 model at the substitution position of the $R_2$ group.

**Table 4**. The variables derived from the pharmacophore generated from our series of the training set.

| Hypo-thesis | RMSD [a] | $R^2$ [b] | Total Costs[c] | Costs Diff.[d] | Closest Random[e] | Features f |
|---|---|---|---|---|---|---|
| Hypo1 | 1.575 | 0.89 | 130.5 | 130.3 | 185.2 | HBA-LI, HBA-LI, HYD-Ar, Ar |
| Hypo2 | 1.777 | 0.86 | 138.0 | 122.8 | 192.9 | HBA-LI, HBA-LI, HBA-LI |
| Hypo3 | 1.818 | 0.85 | 140.7 | 120.1 | 204.4 | HBA-LI, HBA-LI, HYD-Ar |
| Hypo4 | 1.880 | 0.84 | 143.3 | 117.5 | 205.2 | HBA-LI, HBA-LI, HYD-Ar |
| Hypo5 | 1.918 | 0.84 | 143.5 | 117.3 | 208.7 | HBA-LI, HBA-LI, HBA-LI, HYD-Ar |
| Hypo6 | 1.960 | 0.83 | 146.1 | 114.7 | 214.5 | HBA-LI, HBA-LI, HYD-Ar |
| Hypo7 | 2.287 | 0.76 | 165.8 | 95.0 | 218.5 | HBA-LI, HBA-LI, Ar |
| Hypo8 | 2.279 | 0.76 | 168.9 | 91.9 | 219.1 | HBA-LI, HBA-LI, Ar |
| Hypo9 | 2.339 | 0.75 | 169.3 | 91.5 | 219.1 | HBA-LI, HBA-LI, HYD-Ar |
| Hypo10 | 2.442 | 0.72 | 176.4 | 84.4 | 219.4 | HBA-LI, HBA-LI, HYD-Ar |
| Fixedcost | 0 | 1.00 | 89.9 | 170.9 | | |
| Nullcost | 3.537 | 0 | 260.8 | 0 | | |

[a] root mean square deviation (RMSD); [b] squared correlation coefficient; [c] overall cost parameter of the PH4 pharmacophore. [d] cost difference between Null cost and total cost of this hypothesis; [e] lowest cost of 49 scrambled runs (Y) at a selected level of confidence of S = 98%. Fixed Cost = 89.9 with RMSD = 0, Null Cost =260.8 with RMSD = 3.537 and Configuration cost = 9,40. [f] HBA (hydrogen-bond Acceptor); HYD (Hydrophobic); HYD-AL (Hydrophobic Aliphatic); HYD-Ar (Hydrophobic Aromatic); Ar (Ring-aromatic). Number of hypotheses with total cost < Hypo1 cost (=130.5): X=0. S=[1-(1 + X)/Y] ×100=[1-(1 + 0)/ (1 + 49)] ×100 = 98%.

### 3.5. Virtual library

The permutation of the fragments R1 and R2-group on the coumarin skeleton led us to a Table 5 (VL). The 351 R-groups inventoried in Table 5, were fixed instead of the R1 and R2-groups of the COU skeleton to generate the combinatorial library of the size: R1 x R2 = 351 x 351=123,201 analogs. This initial diversity library was generated from building blocks (chemicals) listed in the databases of available chemicals [40]To achieve a drug-compliant molecule library, we put a filter and applied rules such as the Lipinski-of-five rule, which gave us the reduced (VL) which guided us to sample a reduced number of acceptable COU for in silico testing. This method produced 67,949 analogs.

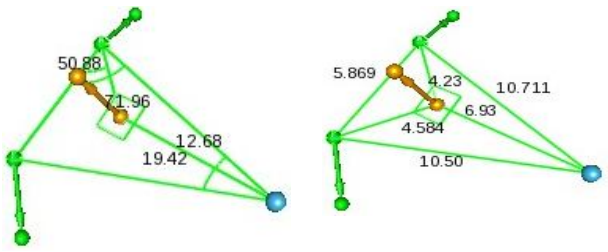

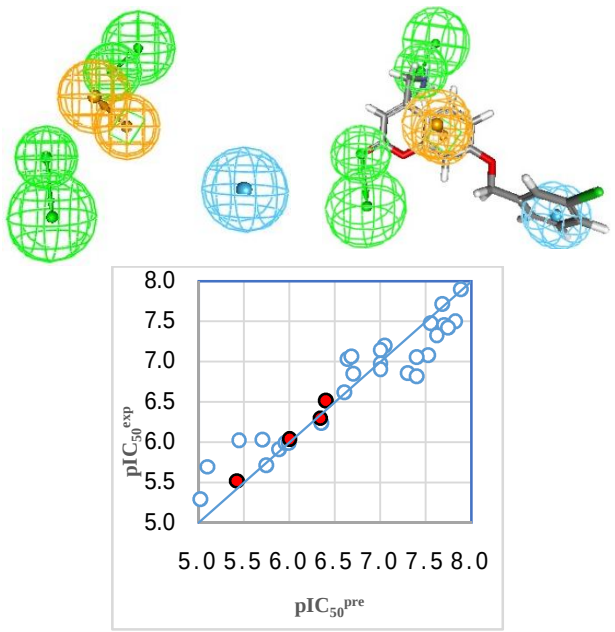


Figure 4. (A, Top left) Angles between centers of pharmacophoric, (B, Top right) distances between centers, (C, Middle left) features coordinates of centers and (D, Middle right) mapping of pharmacophore of MAO-B inhibitor with the most potent molecule COU1. The correlation plot of experimental vs. predicted inhibitory activity is displayed at the left. The features are colored blue for hydrophobic aromatic, green for hydrogen-bond acceptor (HBA) and orange for ring aromatic. The arrows represent the projection for acceptor features. (E, Bottom) Correlation plot of experimental vs predicted inhibitory activity (open square correspond to TS, red square to VS).

### 3.6. *In Silico* Screening of Library of COUs

The focused library of 67,949 COU analogs (COUa)underwent virtual screening for those structures mapping the 3D-QSAR PH4model hypo1 of MAO-B inhibition well. 245 COUs mapped to ≥ 2 features, 50 of them ≥ 4 features. These best fitting COUa (PH4 hits) were submitted to complexation QSAR model evaluation for predicted $IC_{50}^{pre}$. The computed rGFE of MAO-B::COUa complex formation($\Delta\Delta G_{com}$), with $\Delta\Delta H_{MM}$, $\Delta\Delta TS_{vib}$, and $\Delta\Delta G_{sol}$, and $IC_{50}^{pre}$ calculated using Equation B (Table 3) are presented in Table 6.

### 3.7. Novel COU analogs

The creation of a virtual library was obtained on the basis of chemical information such as conformation, interaction etc of the COUs, which was used for the selection of the appropriate R1-and R2-groups. In order to obtain MAO-B candidates with higher predicted inhibitory activity, we analyzed histogram of R1 and R2-groups among the 50 best fit PH4 hits (Fig.5). The histograms show that the R1 group 159, 96 and 250 were represented with the highest frequency of occurrence (5, 3 and 3 respectively) among the 50 COU hits. The R2-groups most frequently represented in this subset are 280(5) and 335(4) with occurrences of 5 and 4 respectively. The top five scoring virtual hits namely, analogs are 96_271 ($IC_{50}^{pre}$ =20 pM), 14_271 ($IC_{50}^{pre}$ =220 pM), 104_249 ($IC_{50}^{pre}$ =420 pM),159_90 ($IC_{50}^{pre}$ =525 pM) and 337_279 ($IC_{50}^{pre}$ =562 pM),). They include the following substituents at $R_1$positon: 159: 4-(5-amino-1H-pyrazol-1-yl)Ph, 96: 2-thio-3,3-diMebutyl and 250: imino(Ph)Me or at R2 position:280: -Bz-2-F and 335: 3-Hydroxy-Benzyl. These R2-groups, all of which are hydropho-bic rings, have a suitable substituent that explores the depth of the hydrophobic pocket. Unlike R2-groups which includes hydrophobic rings, R1-groups have shown a preference for aliphatic substituents.

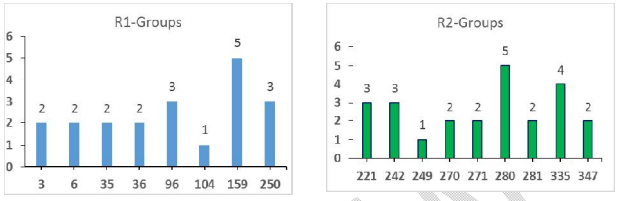


Figure5: Histograms of frequency of occurrence of individual R-groups in the 50 best selected analogs mapping to four features of PH4 pharmacophore hypothesis Hypo1.

### 3.8. Pharmacokinetic profile of novel COU analogs

Obtaining a pharmacokinetic profile of MAO-B inhibitors still requires increased research.Presented in Table 7, the ADME of our new analogs, were described earlier by the QikProp program[41] taken from the method of Jorgensen [42].The fundamental principles of this method are described previously [**Error! Bookmark not defined.**]. Our best analogs are compared with that of drugs used on the market to treat Parkinson's disease. See table 7.

## 4 DISCUSSIONS

The study of MAO-B complexation and coumarin derivatives carried out byBinda *et al.* [43] can still be explored by QSAR. Exploration of MAO_B-COUx complexes shows that hydrophobic interaction plays a key role in significantly enhancing the expected inhibitory potencies. As shown in Fig.6, there is an enhancement of the $E_{int}$ interaction energy with the amino acids in the hydrophobic pocketsurrounded by the following residues: Trp119, Leu164, Leu167, Phe168, Ile198, Ile199, Ile316 and Tyr326 as reported previously [11].Fig.6 displaysin a comparative way this improvement of interaction energy $E_{int}$ with ILE199 and TYR326 known to be the key determinants for binding affinity for the MAO-B inhibitors[6, 7, 8].This structural model, released during PH4 screening of the virtual library of COUs analogues, led to a significant increase in the efficiency of COUs action in $E_{int}$breakdown to MAO_B active site residues when comparing the best TS COU1 (ILE199; -5.2 kcal/mol and Tyr326; -5.1 kcal/mol) to two COUs analogs 96-271 (ILE199; -6.9 kcal/mol and Tyr326; -6.1 kcal/mol) and 14-271 (ILE199; -5.9 kcal/mol and Tyr326; -5.6 kcal/mol) and resulting in stabilization of almost 3 kcal/mol for 96-271 and 1 kcal/mol for 14-271.

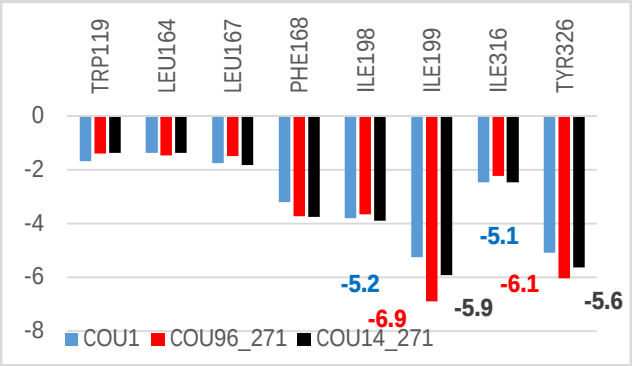


Figure 6Best two novel COU analogs (the color coding refers to ligands given in legend).

## 5. CONCLUSIONS

The inhibition of MAO-B has been assessed successfully through MM-PB QSAR simulations correlating the observed $pIC_{50}$and the computed relative standard Gibbs free energy ofMAO-B:COUs complex formation on the basis of the similarity property principle (SPP) [11].The MAO-B inhibitionsubsequent pharmacophore model (PH4) based on the active conformation of the COUs ligands at the enzyme active site served as chemical space virtual screening tool. The subset of 50 best virtual hits (BVH) identified by the PH4 underwent crosscheck computation of predicted MAO-B inhibitory potencies by the SPP-based QSAR model. The ADME profile of the orally bioavailable novel BVH is favorable compared to current antiparkinsonian compounds. Despite the lack of Molecular Dynamics (MD) runs for stability check of MAO-B:BVHs complexes, theirpredicted $IC_{50}^{pred}$ in the sub nanomolar concentration range encourages the proposal of the following handful of the below-cited analogues to synthesis is worthy.96-271 ($IC_{50}^{pred}$ = 0.1 nM), 14-271 ($IC_{50}^{pred}$ = 0.2nM), 104-249 ($IC_{50}^{pred}$ = 0.4 nM), 337-279 ($IC_{50}^{pred}$ = 0.6 nM) (Table 7), are potential novel potent orally bioavailable antiparkinsonians.

**Table 5** R1-and R2-groups (fragments, building blocks, substituents) used in the design of the initial diversity virtual combinatorial library of coumarin derivatives [27].

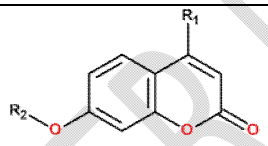


| R-groups [a] | | | | | |
|---|---|---|---|---|---|
| 1 | 1-ClMe-indolizin-7-yl | 2 | ET | 3 | 1-F-ET |
| 4 | propyl | 5 | 1-Brpropyl | 6 | Me-thiol |
| 7 | 1-BrMe | 8 | 1-ClEt | 9 | 1-F-propyl |
| 10 | butyl | 11 | 1-F-Me | 12 | 1-BrEt |
| 13 | 1-Clpropyl | 14 | 1-F-butyl | 15 | 1-Cl-butyl |
| 16 | 1-Clpentyl | 17 | hexyl | 18 | 1-Br-hexyl |
| 19 | isopentyl | 20 | 6,6-diMeheptyl | 21 | 6-Meheptyl |
| 22 | 3,3-diMe-butyl | 23 | 3-Mepentyl | 24 | 6-Meoctyl |
| 25 | 3-Etpentyl | 26 | Me-$C_3H_5$ | 27 | Butyl-$C_3H_5$ |
| 28 | Me-$C_4H_7$ | 29 | Butyl-$C_4H_7$ | 30 | Me-$C_5H_9$ |
| 31 | Butyl-$C_5H_9$ | 32 | Me-$C_6H_{11}$ | 33 | Butyl-$C_6H_{11}$ |
| 34 | cycloprop-2-en-1-yl | 35 | Thiophen-2-yl | 36 | Thiophen-3-yl |
| 37 | Furan-2-yl | 38 | 5-Me-thiophen-2-yl | 39 | 3,4,5-triMe-thiophen-2-yl |
| 40 | Thiophen-2-ylMe | 41 | furan-3-ylMe | 42 | 3-Me-thiophen-2-yl |
| 43 | 3,5-diMe-thiophen-2-yl | 44 | Furan-2-ylMe | 45 | 2-(thiophen-2-yl)Et |
| 46 | 4-Me-thiophen-2-yl | 47 | 4,5-diMe-thiophen-2-yl | 48 | 2-(furan-2-yl)Et |
| 49 | Thiophen-3-ylMe | 50 | Ph | 51 | 4-ClPh |
| 52 | 4-F-Ph | 53 | 4-BrPh | 54 | p-tolyl |
| 55 | 3-F-Ph | 56 | 3-ClPh | 57 | 3-BrPh |
| 58 | m-tolyl | 59 | 2-F-Ph | 60 | 2-ClPh |
| 61 | 2-BrPh | 62 | o-tolyl | 63 | 4-OHPh |
| 64 | 4-MeOPh | 65 | 4-OH-Bn | 66 | 4-MeO-Bn |
| 67 | -Bn | 68 | 4-F-Bn | 69 | 4-Cl-Bn |
| 70 | 4-Br-Bn | 71 | 4-Me-Bn | 72 | 3,5-diMe-Bn |
| 73 | 4-((1H-imidazol-2-yl)Me)-Bn | 74 | aminoMe | 75 | diClMe |
| 76 | 2-(1H-imidazol-2-yl)Et | 77 | 2-clpropyl | 78 | 3-Br-2-(thiazol-2-yl)propyl |
| 79 | (Furan-3-ylMe)thio | 80 | diBrMe | 81 | 2-amino-2-ClEt |
| 82 | 3,3-diBr-3-F-propyl | 83 | 4-(pyridin-3-yl)butyl | 84 | Cl-F-Me |
| 85 | 2-(1,3,4-thiadiazol-2-yl)Et | 86 | 2-Br-2-(1,3,4-thiadiazol-2-yl)Et | 87 | 1-Br-3-Clpropyl |

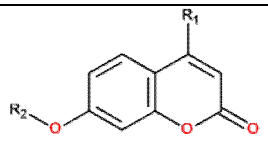


| | R-groups [a] | | | | |
|---|---|---|---|---|---|
| 88 | 4-(1H-imidazol-2-yl)butyl | 89 | 4-Cl-3-OHbutyl | 90 | 3-((F-Me)amino)propyl |
| 91 | 4-OHhexyl | 92 | 6-Br-5-aminohexyl3-((F-Me)amino)propyl | 93 | 4-iodo-3-Mebutyl |
| 94 | 3-(neopentylamino)propyl | 95 | 5-(Meamino)pentyl | 96 | 2-Thio-3,3-diMebutyl |
| 97 | 4-Cl-3-Mepentyl | 98 | 6-aminooctyl | 99 | 4-P-3-Etpentyl |
| 100 | cycloprop-2-en-1-ylMe | 101 | (4-Mecyclohexyl)Me | 102 | 4-Et-Bn |
| 103 | 4-($CF_3$)-Bn | 104 | 3,4-diF-Bn | 105 | 3,5-diF-Bn |
| 106 | 2-Cl-4-F-Bn | 107 | 5-Cl-2-(FMe)-Ph | 108 | 5-Br-2-(FMe)-4-Et-Ph |
| 109 | 3-Me-2($CF_3$)-ph | 110 | 3-F-2(FMe)-ph | 111 | 5-F-2(FMe)-ph |
| 112 | 3,5-diF-2(FMe)-Ph | 113 | 3-(triFMe)pyridin-2-yl | 114 | 2-(triFMe)pyridin-3-yl |
| 115 | 3-(triFMe)pyridin-4-yl | 116 | 3-Br-pyridin-2-yl | 117 | 4-MeO-3-($CF_3$)pyridin-2-yl |
| 118 | 4-($CF_3$)pyridin-3-yl | 119 | 2-($CF_3$)Ph | 120 | EtO |
| 121 | 2-(6-Et-3,6-dihydro-2H-pyran-2-yl)EtO | 122 | 4-(2-F-Pyrrol-1-yl)ph | 123 | 4-(4-F-1H-Pyrazol-1-yl)ph |
| 124 | 4-(3-F-1H-Pyrazol-1-yl)ph | 125 | 4-(4,5-diF-1H-pyrazol-1-yl)Ph | 126 | 4-(3,4,5-triF-1H-pyrazol-1-yl)Ph |
| 127 | 4-(3,4-diF-1H-pyrazol-1-yl)Ph | 128 | 4-(3,5-diF-1H-pyrazol-1-yl)Ph | 129 | 4-(3-Br-1H-pyrazol-1-yl)Ph |
| 130 | 4-(4-Br-1H-pyrazol-1-yl)Ph | 131 | 4-(5-Br-1H-pyrazol-1-yl)Ph | 132 | 4-(4,5-diBr-1H-pyrazol-1-yl)Ph |
| 133 | 4-(3,4-diBr-1H-pyrazol-1-yl)Ph | 134 | 4-(3,5-diBr-1H-pyrazol-1-yl)Ph | 135 | 4-(3,4,5-triBr-1H-pyrazol-1-yl)Ph |
| 136 | 4-(5-Me-1H-pyrazol-1-yl)Ph | 137 | 4-(4-Me-1H-pyrazol-1-yl)Ph | 138 | 4-(3-Me-1H-pyrazol-1-yl)Ph |
| 139 | 4-(3,4-diMe-1H-pyrazol-1-yl)Ph | 140 | 4-(4,5-diMe-1H-pyrazol-1-yl)Ph | 141 | 4-(3,5-diMe-1H-pyrazol-1-yl)Ph |
| 142 | 4-(3,4,5-triMe-1H-pyrazol-1-yl)Ph | 143 | 4-(3-iodo-1H-pyrazol-1-yl)Ph | 144 | 4-(4-iodo-1H-pyrazol-1-yl)Ph |
| 145 | 4-(5-iodo-1H-pyrazol-1-yl)Ph | 146 | 4-(4,5-iodo-1H-pyrazol-1-yl)Ph | 147 | 4-(3,4,-diiodo-1H-pyrazol-1-yl)Ph |
| 148 | 4-(3,4,5-triiodo-1H-pyrazol-1-yl)Ph | 149 | 4-(3,5-diiodo-1H-pyrazol-1-yl)Ph | 150 | 4-(3-Cl-1H-pyrazol-1-yl)Ph |
| 151 | 4-,4-Cl-1H-pyrazol-1-yl)Ph | 152 | 4-(5-Cl-1H-pyrazol-1-yl)Ph | 153 | 4-(4,5-diCl-1H-pyrazol-1-yl)Ph |
| 154 | 4-(3,5-diCl-1H-pyrazol-1-yl)Ph | 155 | 4-(3,4-diCl-1H-pyrazol-1-yl)Ph | 156 | 4-(3,4,5-triCl-1H-pyrazol-1-yl)Ph |
| 157 | 4-(3-amino-1H-pyrazol-1-yl)Ph | 158 | 4-(4-amino-1H-pyrazol-1-yl)Ph | 159 | 4-(5-amino-1H-pyrazol-1-yl)Ph |
| 160 | 4-(4,5-diamino-1H-pyrazol-1-yl)Ph | 161 | 4-(3,5-diamino-1H-pyrazol-1-yl)Ph | 162 | 4-(3,4-diamino-1H-pyrazol-1-yl)Ph |
| 163 | 4-(3,4,5-triamino-1H-pyrazol-1-yl)Ph | 164 | 4-(3-Me-1H-pyrazol-1-yl)Ph | 165 | 4-(4-Me-1H-pyrazol-1-yl)Ph |
| 166 | 4-(5-Me-1H-pyrazol-1-yl)Ph | 167 | 4-(4,5-diMe-1H-pyrazol-1-yl)Ph | 168 | 4-(3,5-diMel-1H-pyrazol-1-yl)Ph |
| 169 | 4-(3,4-diMe-1H-pyrazol-1-yl)Ph | 170 | 4-(3,4,5-triMe-1H-pyrazol-1-yl)Ph | 171 | 4-(5-Et-1H-pyrazol-1-yl)Ph |
| 172 | 4-(4-Et-1H-pyrazol-1-yl)Ph | 173 | 4-(5-Et-4-Me-1H-pyrazol-1-yl)Ph | 174 | 4-(5-Et-3,4-diMe-1H-pyrazol-1-yl)Ph |
| 175 | 4-(5-(Me-Me)-1H-pyrazol-1-yl)Ph | 176 | 4-(5-(Me-Me)-4-Me-1H-pyrazol-1-yl)Ph | 177 | 4-(4,5-di(Me-Me)-1H-pyrazol-1-yl)Ph |
| 178 | 4-(4,5-di(Me-Me)-3-Me-pyrazol-1-yl)Ph | 179 | 4-(5-aminothio-1H-pyrazol-1-yl)Ph | 180 | 4-(4-aminothio-1H-pyrazol-1-yl)Ph |
| 181 | 4-(4-(aminothio)-5-ME-1H-pyrazol-1-yl)Ph | 182 | 4-(4,5-bis(aminothio)-1H-pyrazol-1-yl)Ph | 183 | bisPh-4-yl |
| 184 | 4-(5H-tetrazol-5-yl)Ph | 185 | 4-(Imidazol-1-yl)Ph | 186 | 4-([1,2,4]triazol-1-yl)Ph |
| 187 | 4-(tetrazol-1-yl)Ph | 188 | 4-(thiophen-2-yl)Ph | 189 | 4-(pyridin-2-yl)Ph |
| 190 | 4-(pyrazine-2-yl)Ph | 191 | 4-(pyrimidin-2-yl)Ph | 192 | 4-(pyridazin-3-yl)Ph |
| 193 | 4-(piperazin-1-yl)Ph | 194 | 3H-Indol-2-yl | 195 | 7H-purin-8-yl |
| 196 | 1,8a-dihydro-indolizin-2-yl | 197 | isoquinolin-6-yl | 198 | quinolin-6-yl |
| 199 | cyclopenta-2,4-dienecarbonyl | 200 | 2-Mecyclopenta-2,4-dienecarbonyl | 201 | 2-F-cyclopenta-2,4-dienecarbonyl |
| 202 | 2-amino-cyclopenta-2,4-dienecarbonyl | 203 | 2-Mecyclopenta-2,4-dienecarbonyl | 204 | 3-Mecyclopenta-2,4-dienecarbonyl |
| 205 | 2,3-diMecyclopenta-2,4-dienecarbonyl | 206 | 2-Clcyclopenta-2,4-dienecarbonyl | 207 | 3-Clcyclopenta-2,4-dienecarbonyl |
| 208 | 2,3-diClcyclopenta-2,4-dienecarbonyl | 209 | 3-Brcyclopenta-2,4-dienecarbonyl | 210 | 2-Brcyclopenta-2,4-dienecarbonyl |
| 211 | 2,3-diBrcyclopenta-2,4-dienecarbonyl | 212 | 2-iodocyclopenta-2,4-dienecarbonyl | 213 | 3-iodocyclopenta-2,4-dienecarbonyl |
| 214 | 2,3-dilcyclopenta-2,4-dienecarbonyl | 215 | amino(cyclopenta-2,4-dien-1-yl)Me | 216 | amino(2-F-cyclopenta-2,4-dien-1-yl)Me |
| 217 | amino(2,3-diF-cyclopenta-2,4-dien-1-yl)Me | 218 | amino(2-Me-cyclopenta-2,4-dien-1-yl)Me | 219 | amino(2,3-diMe-cyclopenta-2,4-dien-1-yl)Me |
| 220 | $NH_2$Me(2,3-diMecyclopenta-2,4-dien-1-yl)Me | 221 | $NH_2$Me(2-Me-cyclopenta-2,4-dien-1-yl)Me | 222 | $NH_2$Me(3-Me-cyclopenta-2,4-dien-1-yl)Me |
| 223 | $NH_2$Me(3-F-cyclopenta-2,4-dien-1-yl)Me | 224 | $NH_2$Me(2-F-cyclopenta-2,4-dien-1-yl)Me | 225 | $NH_2$Me(2,3-F-cyclopenta-2,4-dien-1-yl)Me |
| 226 | $NH_2$F(2,3-diMe-cyclopenta-2,4-dien-1-yl)Me | 227 | $NH_2$F(2-Me-cyclopenta-2,4-dien-1-yl)Me | 228 | $NH_2$F(3-Me-cyclopenta-2,4-dien-1-yl)Me |
| 229 | $NH_2$F(3-F-cyclopenta-2,4-dien-1-yl)Me | 230 | $NH_2$F(2,3-diFcyclopenta-2,4-dien-1-yl)Me | 231 | $NH_2$F(2,3-diClcyclopenta-2,4-dien-1-yl)Me |
| 232 | $NH_2$F(2-Clcyclopenta-2,4-dien-1-yl)Me | 233 | $NH_2$F(3-Clcyclopenta-2,4-dien-1-yl)Me | 234 | $NH_2$F(3-Brcyclopenta-2,4-dien-1-yl)Me |
| 235 | $NH_2$F(2,3-diBrcyclopenta-2,4-dien-1-yl)Me | 236 | $NH_2$F(2-Brcyclopenta-2,4-dien-1-yl)Me | 237 | $NH_2$(2-carbamoylcyclo penta-2,4-dien-1-yl)Me |

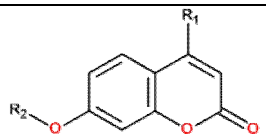

| | R-groups [a] | | | | |
|---|---|---|---|---|---|
| 238 | $NH_2$(3-carbamoylcyclo penta-2,4-dien-1-yl)Me | 239 | $NH_2$(3-F-2carbamoylcyclopenta-2,4-dien-1-yl)Me | 240 | $NH_2$(3-Cl-2-carbamoylcyclopenta-2,4-dien-1- |
| 241 | $NH_2$(3-$NH_2$-2-carbamoylcyclopenta-2,4-dien-1- | 242 | 2-carbamoylPh-$HCOO^-$ | 243 | 3-carbamoylPh-$HCOO^-$ |
| 244 | 4-carbamoylPh-$HCOO^-$ | 245 | 2-MePh-$HCOO^-$ | 246 | 3-MePh-$HCOO^-$ |
| 247 | 4-MePh-$HCOO^-$ | 248 | 2,3-diMePh-$HCOO^-$ | 249 | (2-carbamoylPh)(imino)Me |
| 250 | imino(Ph)Me | 251 | (3-carbamoylPh)(imino)Me | 252 | 4-carbamoylPh(imino)Me |
| 253 | 2-MePh(imino)Me | 254 | 2,3-diMePh(imino)Me | 255 | 3-MePh(imino)Me |
| 256 | 4-MePh(imino)Me | 257 | 2-FPh(imino)Me | 258 | 3-FPh(imino)Me |
| 259 | 3-BrPh(imino)Me | 260 | 2-BrPh(imino)Me | 261 | 2-ClPh(imino)Me |
| 262 | 3-ClPh(imino)Me | 263 | (3-ClPh)(Br-imino)Me | 264 | (3-BrPh)(Br-imino)Me |
| 265 | (3-ClPh)(Cl-imino)Me | 266 | (2-ClPh)(Cl-imino)Me | 267 | (2-MePh)(-imino)Me |
| 268 | imino(2-($CF_3$)Ph)Me | 269 | imino(3-($CF_3$)Ph)Me | 270 | 3-formylbenzamide |
| 271 | 2-formylbenzamide | 272 | 4-formylbenzamide | 273 | -Bz-2-thiol |
| 274 | -Bz-2,3-diMe | 275 | -Bz-3-Me | 276 | -Bz-4-Me |
| 277 | -Bz-2-Me | 278 | -Bz-2-($CF_3$) | 279 | -Bz-3-($CF_3$) |
| 280 | -Bz-2-F | 281 | $NH_2$(3-Br-2-carbamoylcyclopenta-2,4-dien-1-yl)Me | 282 | Carbamoyl |
| 283 | 4-Cl-1H-pyrazol-1-yl | 284 | 4,5-diCl-1H-pyrazol-1-yl | 285 | 5-Cl-1H-pyrazol-1-yl |
| 286 | 3-Cl-1H-pyrazol-1-yl | 287 | 3-Br-1H-pyrazol-1-yl | 288 | 4-Br-1H-pyrazol-1-yl |
| 289 | 5-Br-1H-pyrazol-1-yl | 290 | 4,5-diBr-1H-pyrazol-1-yl | 291 | 3,4,5-triBr-1H-pyrazol-1-yl |
| 292 | 4-Me-1H-pyrazol-1-yl | 293 | 4,5-diMe-1H-pyrazol-1-yl | 294 | 5-Me-1H-pyrazol-1-yl |
| 295 | 5-iodo-1H-pyrazol-1-yl | 296 | 4-iodo-1H-pyrazol-1-yl | 297 | 3-iodo-1H-pyrazol-1-yl |
| 298 | 3,4-diI-1H-pyrazol-1-yl | 299 | 3,4,5-triiodo-1H-pyrazol-1-yl | 300 | 3,4-diF-1H-pyrazol-1-yl |
| 301 | 3-F-1H-pyrazol-1-yl | 302 | 1,3-diF-1H-pyrazol-1-yl | 303 | 1-F-1H-pyrazol-1-yl |
| 304 | 1-F-1H-pyrazol-2-yl | 305 | 3-amino-1H-pyrazol-1-yl | 306 | 4-amino-1H-pyrazol-1-yl |
| 307 | 5-amino-1H-pyrazol-1-yl | 308 | 5-Me-1H-pyrazol-1-yl | 309 | 5-Et-1H-pyrazol-1-yl |
| 310 | 4-Me-1H-pyrazol-1-yl | 311 | 4,5-diMe-1H-pyrazol-1-yl | 312 | 5-(Me-Me)-1H-pyrazol-1-yl |
| 313 | 4-Me-5-(Me-Me)-1H-pyrazol-1-yl | 314 | 5-($H_2N$-thio)-4-Me-1H-pyrazol-1-yl | 315 | 4,5-bis(aminothio)-1H-pyrazol-1-yl |
| 316 | 4,5-bis( $H_2N$-thio)-3-Me-1H-pyrazol-1-yl | 317 | 5-Et-3-Me-1H-pyrazol-1-yl | 318 | pyridazin-3-yl |
| 319 | pyridazin-4-yl | 320 | pyrimidin-4-yl | 321 | 1,3,5-triazin-2-yl |
| 322 | pyrimidin-2-yl | 323 | pyrazin-2-yl | 324 | Cyclohexyl |
| 325 | piperazin-1-yl | 326 | tetrahydropyridazin-1(2H)-yl | 327 | piperazin-1-yl |
| 328 | 3-Cl-benzyl | 329 | Me-amino-Me | 330 | 2-amino-Et |
| 331 | Aceticacid | 332 | Benzoicacid | 333 | 2-F-2-(1-Me-ureido)-acetamide |
| 334 | 4-tert-butyl-benzoic acid | 335 | 3-Hydroxy-Benzyl | 336 | Benzyloxy-(3-br-propyl)$NH_2$-Me |
| 337 | Propionicacid | 338 | dipropylaminomethyl | 339 | (3-br-propyl)ph-amino Me |
| 340 | [(Bromo-Me-Me sulfanyl-amino)-Me] | 341 | Bis(Me-Me)-amino Me | 342 | Me-urea |
| 343 | hydroxyaminomethyl | 344 | urea | 345 | (cyclohexyl-3-Et-pentyl)-amino-Me |
| 346 | Acetamide | 347 | 3-Cl-Me-benzyl | 348 | 3-Cl-5-Me-benzyl |
| 349 | 3-propyl-benzyl | 350 | 3-bromomethyl-benzyl | 351 | hydroxy |

[a] All fragments were used for substitutions in the $R_1$ and $R_2$ positions.

**Table 6**rGFE$\Delta\Delta G_{com}$ = $\Delta\Delta H_{MM}$ + $\Delta\Delta G_{sol}$ – $\Delta\Delta TS_{vib}$for the top scoring 50 virtual COU analogs. For analogname the R1 and R2 indexes of substituent numbers come from Table 5.

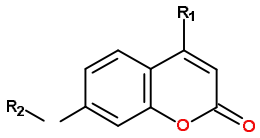

| N° | Designed[a] Analogues | $M_w$[a] | $\Delta\Delta H_{MM}$[b] | $\Delta\Delta G_{sol}$[c] | $\Delta\Delta TS_{vib}$[d] | $\Delta\Delta G_{com}$[e] | $IC_{50}^{pred}$ [f][nM] |
|---|---|---|---|---|---|---|---|
| - | COU1 | 329.8 | 0.0 | 0.0 | 0.0 | 0.0 | 13 [g] |
| 1 | 298-335 | 492.1 | -4.2 | 4.2 | -4.0 | 4.0 | 144.4 |
| 2 | 204-280 | 408.4 | -29.9 | 25.4 | -4.8 | 0.3 | 21.7 |
| 3 | 337-279 | 406.3 | -20.5 | 7.6 | -6.0 | -6.9 | 0.6 |
| 4 | 346-347 | 371.1 | -2.6 | 0.3 | -1.7 | -0.6 | 13.7 |
| 5 | 250-280 | 387.4 | -10.9 | 7.3 | -4.2 | 0.6 | 25.6 |
| 6 | 344-347 | 372.8 | -6.9 | 1.3 | -2.7 | -2.8 | 4.4 |
| 7 | 247-335 | 420.4 | -11.7 | 11.3 | -5.9 | 5.5 | 303.5 |

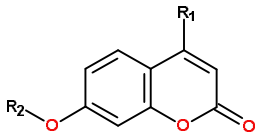

| N° | Designed[a] Analogues | $M_w$[a] | $\Delta\Delta H_{MM}$[b] | $\Delta\Delta G_{sol}$[c] | $\Delta\Delta TS_{vib}$[d] | $\Delta\Delta G_{com}$[e] | $IC_{50}^{pred}$[f] [nM] |
|---|---|---|---|---|---|---|---|
| 8 | 250-221 | 422.5 | -5.3 | 9.7 | -1.3 | 5.7 | 336.9 |
| 9 | 306-70 | 412.2 | -1.6 | 2.4 | -0.9 | 1.7 | 45.1 |
| 10 | 344-106 | 344.8 | -0.2 | 2.1 | -4.4 | 6.3 | 465.1 |
| 11 | 301-273 | 382.4 | -1.5 | 2.9 | -2.8 | 4.2 | 156.1 |
| 12 | 250-91 | 393.4 | -12.5 | 8.4 | -1.6 | -2.5 | 5.2 |
| 13 | 275-222 | 455.6 | -5.9 | 14.5 | 0.1 | 8.5 | 1367.2 |
| 14 | 273-196 | 429.5 | -7.3 | 8.8 | -2.5 | 4.0 | 142 |
| 15 | 35-280 | 366.4 | -6.9 | 3.9 | -3.1 | 0.1 | 19.9 |
| 16 | 238-85 | 410.5 | -20.2 | 12.2 | -2.9 | -5.0 | 1.4 |
| 17 | 243-250 | 428.4 | -10.7 | 11.4 | -6.1 | 6.8 | 602.4 |
| 18 | 1-238 | 463.9 | -17.8 | 18.6 | -0.2 | 1.1 | 33.2 |
| 19 | 6-278 | 380.3 | -0.1 | 2.5 | -5.0 | 7.4 | 798.6 |
| 20 | 6-339 | 434.4 | 1.3 | 2.6 | 0.0 | 3.9 | 136 |
| 21 | 47-272 | 419.5 | 2.3 | 3.9 | -2.6 | 8.9 | 1719 |
| 22 | 71-333 | 413.4 | -17.9 | 9.2 | -1.7 | -6.8 | 0.6 |
| 23 | 85-280 | 396.4 | -0.1 | -0.4 | -5.5 | 4.9 | 231.7 |
| 24 | 2-242 | 353.3 | -2.3 | 5.7 | -1.4 | 4.8 | 214.6 |
| 25 | 14-271 | 383.4 | -25.6 | 15.5 | -1.3 | -8.7 | 0.2 |
| 26 | 96-271 | 425.5 | -17.9 | 6.1 | 1.3 | -13.2 | 0.1 |
| 27 | 79-205 | 430.5 | -19.5 | 12.4 | -7.7 | 0.6 | 25.9 |
| 28 | 35-335 | 350.4 | -6.6 | 4.5 | 0.4 | -2.4 | 5.4 |
| 29 | 96-270 | 425.5 | -13.9 | 8.3 | 0.5 | -6.2 | 0.8 |
| 30 | 102-163 | 467.5 | -42.4 | 47.8 | -1.3 | 6.7 | 555.5 |
| 31 | 294-267 | 377.4 | 7.0 | -0.9 | -0.1 | 6.2 | 439.6 |
| 32 | 104-249 | 434.4 | -20.6 | 8.5 | -4.5 | -7.5 | 0.4 |
| 33 | 89-242 | 431.8 | -2.7 | 3.0 | -2.1 | 2.4 | 63 |
| 34 | 91-64 | 368.4 | -21.5 | 24.8 | 1.7 | 1.5 | 40.7 |
| 35 | 163-281 | 564.4 | -21.1 | 24.6 | -2.1 | 5.6 | 316.6 |
| 36 | 96-281 | 493.4 | -17.2 | 16.9 | 3.5 | -3.8 | 2.7 |
| 37 | 277-239 | 434.4 | 2.9 | 2.8 | -3.6 | 9.3 | 2089.3 |
| 38 | 36-240 | 414.9 | -1.0 | 6.4 | -2.9 | 8.2 | 1202.3 |
| 39 | 3-221 | 365.4 | 6.4 | 3.4 | 2.7 | 7.0 | 660 |
| 40 | 3-216 | 319.3 | 0.6 | 4.1 | -0.2 | 4.9 | 230 |
| 41 | 37-92 | 406.3 | 8.2 | 2.5 | 4.1 | 6.6 | 530 |
| 42 | 36-242 | 407.4 | -9.9 | 7.6 | -3.7 | 1.5 | 40 |
| 43 | 314-335 | 413.5 | 5.5 | 1.1 | -1.9 | 8.5 | 1420 |
| 44 | 201-280 | 394.3 | -34.4 | 24.7 | -5.4 | -4.2 | 2.2 |
| 45 | 158-221 | 476.6 | -17.5 | 12.1 | 0.3 | -5.6 | 1.1 |
| 46 | 159-270 | 466.5 | -26.7 | 18.7 | -5.2 | -2.7 | 4.7 |
| 47 | 159-90 | 408.4 | -25.3 | 17.3 | -0.9 | -7.0 | 0.5 |
| 48 | 159-94 | 446.5 | -21.0 | 14.8 | -0.5 | -6.7 | 0.6 |
| 49 | 159-117 | 494.4 | -16.4 | 15.4 | -6.2 | 5.2 | 270 |
| 50 | 159-79 | 431.5 | -17.4 | 21.6 | -4.3 | 8.4 | 1370 |

[a] $M_w$[g.mol$^{-1}$] is the molecular mass of inhibitors ; [b] $\Delta\Delta H_{MM}$[kcal.mol$^{-1}$] is the relative enthalpic contribution to the Gibbs free energy change related to enzyme-inhibitor (E:I) complex formation $\Delta\Delta G_{com}$ (for details see footnote pf Table 2); [c] $\Delta\Delta G_{sol}$[kcal.mol$^{-1}$] is the relative solvation Gibbs free energy contribution to $\Delta\Delta G_{com}$; [d] $\Delta\Delta TS_{vib}$[kcal.mol$^{-1}$] is the relative(vibrational) entropic contribution to $\Delta\Delta G_{com}$ ; [e] $\Delta\Delta G_{com}$[kcal.mol$^{-1}$] is the relative Gibbs free energy change related to the enzyme-inhibitor MAO-B:: COU complex formation $\Delta\Delta G_{com} \cong \Delta\Delta H_{MM} + \Delta\Delta G_{sol} - \Delta\Delta TS_{vib}$; [f] $IC_{50}^{pre}$ is the predicted inhibition potency MAO-B inhibitors calculated from $\Delta\Delta G_{com}$ using correlation B; Table 3; [g]$IC_{50}^{exp}$[nM] is given for the reference inhibitor COU1 instead of the $IC_{50}^{pre}$.

**Table 7** Predicted ADME-related properties of the best designed COU analogues and known Parkinson agents either in clinical.

| COUx[a] | #stars[b] | $M_W$[c] | $S_{mol}$[d] | $S_{mol/hfo}$[e] | $V_{mol}$[f] | RotB[g] | $HB_{don}$[h] | $HB_{acc}$[i] | $logP_{o/w}$[j] | $logS_{wat}$[k] | logKHsa[l] | PlogB/B[m] | BIPcaco[n] | #meta[o] | $IC50^{pre}$[p] (nM) | HOA[q] | %HOA[r] |
|---|---|---|---|---|---|---|---|---|---|---|---|---|---|---|---|---|---|
| 337-279 | 0 | 406.3 | 649.5 | 109.7 | 1140.3 | 4 | 0 | 7.5 | 2.8 | -4.4 | -0.2 | -0.9 | 319.2 | 2 | 0.6 | 3 | 87.9 |
| 344-347 | 0 | 372.8 | 636.4 | 123.7 | 1111.8 | 5 | 3 | 5.2 | 2.3 | -3.6 | -0.0 | -1.5 | 57.9 | 4 | 4.4 | 3 | 87.8 |
| 250-91 | 0 | 393.4 | 711.4 | 214.4 | 1271.2 | 10 | 2 | 7.7 | 2.9 | -4.7 | 0.1 | -2.1 | 121.2 | 2 | 5.2 | 3 | 81.0 |
| 238-85 | 0 | 410.4 | 669.2 | 108.5 | 1192.7 | 8 | 4 | 8.7 | 0.8 | -3.0 | -0.2 | -2.1 | 6.2 | 8 | 1.4 | 2 | 83.9 |
| 71-333 | 0 | 413.4 | 695.4 | 194.3 | 1241.0 | 6 | 3 | 7.5 | 1.1 | -2.8 | -0.4 | -2.1 | 14.4 | 4 | 0.6 | 2 | 84.4 |
| 14-271 | 0 | 383.4 | 668.2 | 152.7 | 1172.1 | 6 | 2 | 7.5 | 2.5 | -4.9 | 0.0 | -1.7 | 141.2 | 2 | 0.2 | 3 | 80.2 |
| 96-271 | 0 | 425.5 | 699.4 | 183.9 | 1272.8 | 7 | 2.8 | 8 | 2.9 | -5.1 | 0.1 | -1.6 | 145.3 | 3 | 0.0 | 3 | 82.6 |
| 35-335 | 0 | 350.4 | 608.2 | 29.1 | 1054.3 | 4 | 1 | 4 | 3.9 | -5.4 | 0.5 | -0.8 | 629.5 | 4 | 5.4 | 3 | 100 |
| 96-270 | 0 | 425. | 705. | 184.0 | 1282. | 7 | 2.8 | 8 | 2.7 | -5.2 | 0.2 | -1.9 | 85.6 | 3 | 0.8 | 3 | 85. |

| | | | | | | | | | | | | | | | | | |
|---|---|---|---|---|---|---|---|---|---|---|---|---|---|---|---|---|---|
| 104-249 | 0 | 5<br>434.4 | 9<br>689.3 | 35.9 | 2<br>1237.9 | 7 | 3 | 6.5 | 3.5 | -5.5 | 0.3 | -1.5 | 154.6 | 2 | 0.4 | 3 | 6<br>86.6 |
| 96-281 | 0 | 493.4 | 711.8 | 215.2 | 1307.8 | 9 | 4.8 | 7.2 | 2.6 | -4.0 | 0.1 | -1.3 | 31.6 | 7 | 2.7 | 2 | 69.0 |
| Rasagiline | 2 | 173.3 | 417.1 | 210.6 | 675.1 | 4 | 1.5 | 1.5 | 2.3 | -1.3 | -0.1 | 0.5 | 1562.4 | 5 | | 3 | 100 |
| Lazabemide | 0 | 199.6 | 400.9 | 74.6 | 643.5 | 4 | 3 | 4.5 | 0.1 | -0.6 | -0.5 | -0.3 | 96.9 | 3 | | 2 | 63.1 |
| Safinamide | 0 | 302.3 | 575.7 | 168.0 | 998.0 | 7 | 3 | 4.7 | 1.8 | -1.6 | -0.3 | -0.3 | 139.2 | 6 | | 3 | 75.9 |

[a] designed TKI analogues (Table 6) and known anti tuberculosis; [b] drug-likeness, number of property descriptors (24 of the full list of 49 QikProp descriptors, ver. 6.5, release 139) that fall outside the *range of values for 95% of known drugs*; [c] molar mass in [g.mol$^{-1}$] (*range for 95% of drugs: 130–725 g mol$^{-1}$*) [44]; [d] total solvent-accessible molecular surface, in (Å2) (probe radius 1.4 Å) (*300–1000 Å2*); [e] hydrophobic portion of the solvent-accessible molecular surface, in (Å$^2$) (*0–750 Å$^2$*); [f] total volume of the molecule enclosed by solvent-accessible molecular surface, in (Å$^3$) (*500–2000 Å$^3$*); [g] number of rotatable non-trivial (not CX3), non-hindered (not alkene, amide, small ring) bonds (*0–15*); [h] estimated number of hydrogen bonds that would be donated by the solute to water molecules in an aqueous solution. Values are averages taken over a number of configurations, so they can assume non-integer values (*0.0–6.0*); [i] estimated number of hydrogen bonds that would be accepted by the solute from water molecules in an aqueous solution (*2.0–20.0*); [j] logarithm of the partition coefficient between the n-octanol and water phases (*-2 to 6.5*); [k] logarithm of predicted aqueous solubility, logS. S in (mol.dm$^{-3}$) is the concentration of the solute in a saturated solution that is in equilibrium with the crystalline solid (*-6.0 to 0.5*); [l] logarithm of the predicted binding constant to human serum albumin (*-1.5 to 1.5*); [m] logarithm of the predicted brain/blood partition coefficient (*-3.0 to 1.2*); [n] predicted apparent Caco-2 cell membrane permeability on the Boehringer–Ingelheim scale in [nm.s$^{-1}$] (*<25 poor, >500 nm s$^{-1}$ great*); [o] number of likely metabolic reactions (*1–8*); [p] predicted inhibition constants $IC_{50}^{pre}$ of designed TKIs vs. *Mtb* Thymidylate kinase.; [q] human oral absorption (*1 = low, 2 = medium, 3 = high*); [r] percentage of human oral absorption in the gastrointestinal tract (*<25% = poor, >80% = high*); * star in any column indicates that the property descriptor value of the compound falls outside *the range of values for 95% of known drugs*.

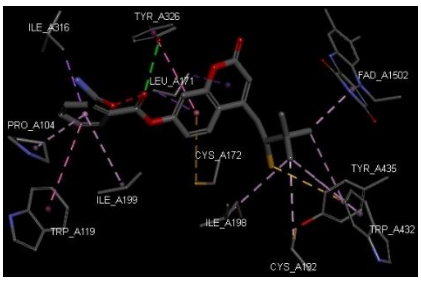


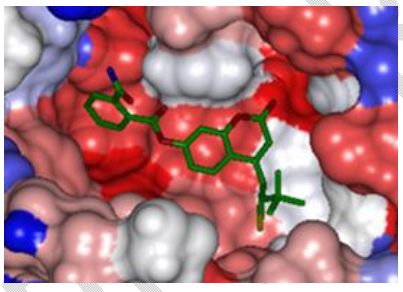

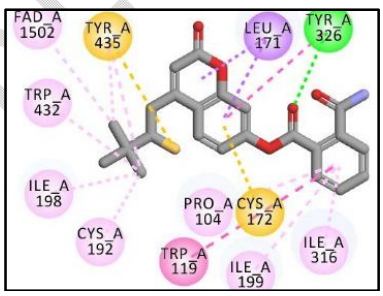


96-271

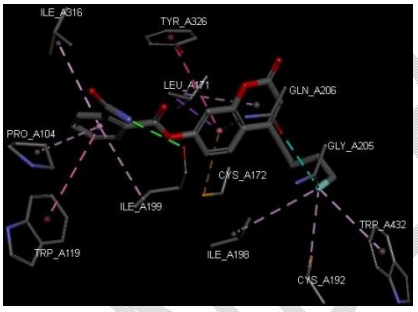


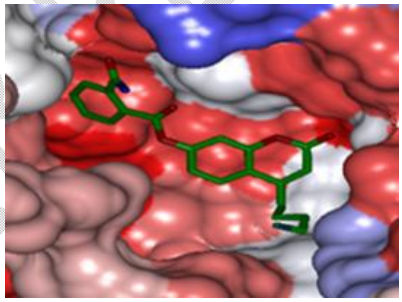

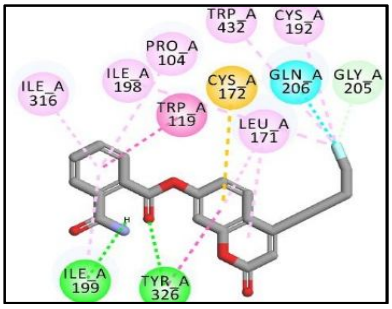


14-271

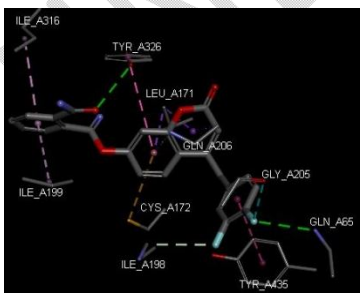


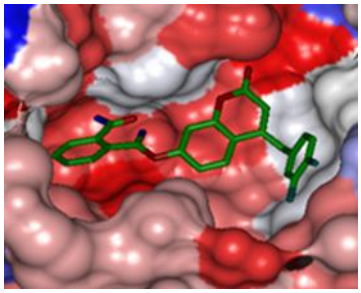

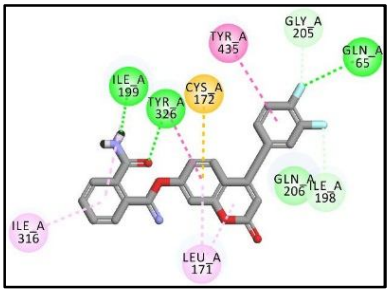


104-249

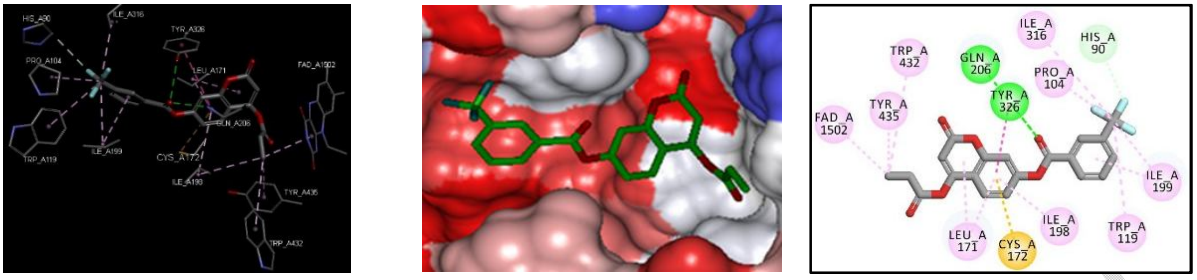


337-279

**Figure 7: The** virtual hit 96-271, 14-271, 104-249, 337-279. The most active designed COU analogs at the active site of MAO-B (3D).2D schematic interaction diagram of the most active designed COU analogs.Connolly Surface of the active site of MAO-B for 4 best active designed COU analogs. The binding site surface is colored according to residue hydrophobicity: red = hydrophobic, blue = hydrophilic and white = intermediate

**ABBREVIATIONS**

2D : Two-dimensional
3D : Three-dimensional
ADME : Absorption, distribution, metabolism, and excretion
MAO-B : Monoamine Oxidase B
hMAO-B : Human Monoamine Oxidase B
hMAO-A : Human Monoamine Oxidase A
COUx : Training set of Coumarins derivatives
COU:Coumarins derivatives
$\Delta\Delta G_{com}$ : Relative complexation GFE
GFE : Gibbs free energy
VL : Virtual Library
VCL : Virtual Combinatorial Library
$\Delta\Delta G_{sol}$ : Relative solvation GFE
HBA : Hydrogen bond Acceptor
HBD : Hydrogen bond Donor
HMM : Enthalpy component of GFE
IC50 : Half-maximal inhibitory concentration
$K_i$ : inhibitory concentration
HOA : Human oral absorption
HYD : Hydrophobic
HYDA : Hydrophobic Aliphatic
MM : Molecular mechanics
MM-PB : Molecular mechanics–Poisson–Boltzmann
PDB : Protein Data Bank
PH4 : Pharmacophore
QSAR : Quantitative structure–activity relationships
RMSD : Root-mean square deviation
D.S. 2.5 : Discovery Studio 2.5
TS : Training set
VS : Validation set

## References


1. Strolin B. M., Tipton K. F., Whomsley R. Amine oxidases and monooxygenases in the in vivo metabolism of xenobiotic amines in humans: has the involvement of amine oxidases been neglected? *Fundam Clin Pharmacol.* **2007**; 21(5):467-80. doi: 10.1111/j.1472-8206.2007.00498.x

2. Shih J. C., Chen K., Ridd M. J., Monoamine oxidase: from genes to behavior. *Annu Rev Neurosci.* **1999**; 22:197-217. doi:10.1146/annurev.neuro.22.1.197.

3. Edmondson D. E., Binda C., Wang J., Upadhyay A. K., Mattevi A. Molecular and mechanistic properties of the membrane-bound mitochondrial monoamine oxidases. *Biochem*. **2009**, 48, 4220-4230. https://doi.org/10.1021 /bi900413g.

4. Bortolato M., Chen K., Shih J. C., Monoamine oxidase inactivation: from pathophysiology to therapeutics. *Adv Drug Deliv Rev.***2008**; 60(13-14): 1527-33. https:// doi.org/10. 1016/j.addr.2008.06.002.

5. Lawrence M. S., George P., and Mark A. S., *Chemical Res. Toxicol.***2008** *21* (1), 172-188 DOI:10.1021/tx700210j.

6. Tsugeno Y, Ito A. A key amino acid responsible for substrate selectivity of monoamine oxidase A and B. *J Biol Chem.* **1997,** 272(22):14033-6. doi: 10.1074/jbc.272.22.14033

7. Hubalek F., Binda C., Khalil A., Li M., Mattevi A., Castagnoli N., & Edmondson D. E. Demonstration of isoleucine 199 as a structural determinant for the selective inhibition of human monoamine oxidase B by specific reversible inhibitors. *J.Biol. Chem*. **2005**, 280, 15761-15766.

8. Geha R. M., Rebrin I., Chen K., & Shih J. C. Substrate and inhibitor specificities for human monoamine oxidase A and B are influenced by a single amino acid. *J. Biol*. **2001**, 276, 9877-9882.

9. Li M., Binda C., Mattevi A., & Edmondson D. E. Functional role of the 'aromatic cage' in human monoamine oxidase B: Structures and catalytic properties of Tyr 435 mutant proteins. *Biochemistry***2006**, 45, 4775-4784.

10. Binda C., Wang J., Pisani L., Caccia C., Carotti A., Salvati P., Edmondson D., Mattevi A. Structures of human monoamine oxidase B complexes with selective noncovalent inhibitors : safinamide and coumarin analogs. *J. Med. Chem*. **2007**, 50, 5848-5852.

11. Leonardo P., Giovanni M., Teresa F. M., Orazio N., Francesco L., Marco C., Carla C., Patricia S., Ramon S.O., Estefania M. A., Celine P., & Angelo C. Discovery of a Novel Class of Potent Coumarin Monoamine Oxidase B Inhibitors. **2009**, *J. Med. Chem*. 52, 6685-6706. https://doi.org/10. 1021/jm9010127.

12. Youdim M. B.H., Gross A.and Finberg J.P.M. Rasagiline [N-propargyl-1R(+)-aminoindan], a selective and potent inhibitor of mitochondrial monoamine oxidase B. **2001**, British *J. Pharmacol.* 132, 500-506. DOI:10.1038/sj.bjp.0703826

13. Saura J., Kettler R., Da Prada M., and Richards J. G. Quantitative Enzyme Radioautography with 3H-Ro 41-I 049 and 3H-Ro 19-6327 in vitro: Localization and Abundance of MAO-A and MAO-B in Rat CNS, Peripheral Organs, and Human Brain. **1992**, *J. Neurosci*, 12(5): 1977-1999. DOI: 10.1523/JNEUROSCI.12-05-01977.1992

14. Binda C., Wang J.,Pisani L., Caccia C., Carotti A., Salvati P., Edmondson D. E., and Mattevi A. Structures of Human Monoamine Oxidase B Complexes with Selective Noncovalent Inhibitors:Safinamide and Coumarin Analogs. **2007**, *J. Med. Chem.*, 50, 5848-5852.DOI: 10.1021/jm070677y

15. Berman H. M., Westbrook J., Feng Z., Gilliland G., Bhat T. N., Wessig H., Shindyalov I. N., Bourne P. E. The protein data bank. *Nucl. Acids Res*. **2000**, 28, 235-242.

16. Discovery Studio molecular modeling and simulation program version 2.5, Accelrys, Inc., San Diego, CA, 92121, USA, **2009.**

17. Owono Owono L. C., Keita M., Megnassan E., Frecer V. & Miertus S. Design of Thymidine Analogues Targeting Thymidilate Kinase of Mycobacterium tuberculosis. *Tuberculosis research and treatment*, **2013**, 670836. https://doi.org/10.1155/2013/670836.

18. Frecer V., Miertus S., Tossi A. & Romeo D. Rational design of inhibitors for drug-resistant HIV-1 aspartic protease mutants. *Drug Des. Discov.*, **1998**,15(4), 211-231.

19. Frecer V., Miertus S. Interactions of ligands with macromole-cules: rational design of specific inhibitors of aspartic protea-se of HIV-1. *Macromol Chem Phys*; **2002,** 203: 1650–1657 https://doi.org/10.1002/1521-3935(200207)203:10/11<1650::AID-MACP1650>3.0.CO;2-E

20. Frecer V., Berti F., Benedetti F. & Miertus S. Design of peptidomimetic inhibitors of aspartic protease of HIV-1 containing -Phe Psi Pro- core and displaying favourable ADME-related properties. *J. Mol. Graph Model*, **2008**, 27 (3), 376-387. https://doi.org/10.1016/j.jmgm.2008. 06.006.

21. Dali B., Keita M., Megnassan E., Frecer V. & Miertus S. Insight into selectivity of peptidomimetic inhibitors with modified statine core for plasmepsin II of plasmodium falciparum over human cathepsin D. Chem. *Biol. Drug Des*. **2012**, 79 (4), 411-430. https://doi.org/10.1111/ j.1747-0285.2011.01276.x.

22. Megnassan E., Keita M., Bieri C., Esmel A., Frecer V. & Miertus S. Design of novel dihydroxynaphthoic acid inhibitors of plasmodium falciparum lactate dehydrogenase. *Med. Chem*. **2012**, 8(5), 970-984.

23. Keita M., Kumar A., Dali B., Megnassan E., Siddiqi M. I., Frecer V. and Miertus S. Quantitative Structure-activity relationships and design of thymine-like inhibitors of thyme-dine monophosphate kinase of *Mycobacterium tuberculosis* with favourable pharmacokinetic profiles. *RSC Adv.*, **2014**, 4(99), 55853-55866. https://doi.org/10.1039/c4ra06917j.

24. Owono Owono L. C., Ntie-Kang F., Keita M., Megnassan E., Frecer V. and Miertus S. Virtually Designed Triclosan-Based Inhibitors of Enoyl-Acyl Carrier Protein Reductase of Mycobaterium tuberculosis and of Plasmodium falciparum. *Mol. Inform.*, (2015) 34(5), 292-307. https://doi.org/10.1002/minf.201400141.

25. Kouassi A. F., Kone M., Keita M., Esmel A., Megnassan E., N'Guessan Y. T., & Miertus S. Computer-Aided Design of orally Biovailable

pyrrolidine Carboxamide Inhibitors of Mycobacterium turberculosis with Favorable Pharmaco-kinetic Profiles. *Int. J. Mol. Sci*, (**2015**). 16 (12), 29744-29771. https://doi.org/10.3390/ ijms161226196.

26. Allangba K. N. P. G., Keita M.,Kre N'Guessan R., Megnassan E., Vladimir F., Miertus S. Virtual design of novel *Plasmodium falciparum* cysteine protease falcipain-2 hybrid lactone–chalcone and isatin–chalcone inhibitors probing the S2 active site pocket, *Journal of Enzyme Inhibition and Medicinal Chemistry*, **2019**, 34:1, 547-561.https://doi.org/10.1080/14756366.2018.1564288

27. Kouman K. C., Keita M., N'Guessan K. R., Owono Owono L.C., Megnassan E., Vladimir F. & Miertus S., Structure-Based Design and *in silico* Screening of Virtual Combinatorial Library of Benzamides Inhibiting 2-trans Enoyl-Acyl Carrier Protein Reductase of *Mycobacterium tuberculosis* with Favorable Predicted Pharmacokinetic Profiles. *Int. J. Mol. Sci.*, **2019**, 20, 4730. https://doi.org/10.3390/ijms20194730.

28. N'Guessan, H., Soro, I., Keita, M. and Megnassan, E. "Design and *in silico* Screening of Combinatorial Library of New Herbicidal Analogs of Cycloalka[d]quinazoline-2,4dione-Benzoxazinones Inhibiting Protoporphyrino-gen IX Oxidase", *J. Pharm. Res. Int.*,**2022**, 34(56), pp. 42–61. doi:10.9734/jpri/2022/v34i567251

29 Bernard, D. A. M., Keita, M., Bisseyou, Y. B. M., Esmel, A. and Megnassan, E. "Computer-assisted Design of Novel Polyketide Synthase 13 of Mycobacterium tuberculosis Inhibitors Using Molecular Modeling and Virtual Screening", *J. Pharm. Res. Int.*, **2022**, 34(56), pp. 12–41. doi:10.9734/jpri/2022/v34i567250.

30. Bieri C., Esmel A., Keita M., Owono Owono LC., Dali B., Megnassan E., Frecer V., Miertus S. « Structure-Based Design and Pharmacophore-Based Virtual Screening of Combinatorial Library of Triclosan Analogues Active against Enoyl-Acyl Carrier Protein Reductase of Plasmodium falciparum with Favourable ADME Profiles », *Int. J. Mol. Sci.*, **2023,** 24, (8): 6916. doi:10.3390/ijms24086916.

31. Kone M., N'Guessan H., N'Gouan A. J., M-Koblavi F., Megnassan E. Computer-aied Design of New Hydroxamic Acid Derivatives Targeting the Plasmodium falciparum M17 Metallo-aminopeptidase with Favorable pharmcokinetic Profile. *Int. J. Pharm. Sci. and Drug Res*. **2023**, 15(3) : 356-375. https://doi.org/10.25004/ IJPSDR.2023.150317

32 Ziki E., Akonan L., Kouman K.C., Dali B., Megnassan E.,Kakou-Yao R., Tenon A. J., Frecer V., and Miertus S., Virtual Design of Novel CoumarinylSubstituted Sulfonamide Inhibitors of Carbonic Anhydrase II as Potential Drugs against Glaucoma. *J. Pharm. Res. Int.*, **2023**, 35(24), pp. 10-33. DOI: 10.9734/JPRI/2023/v35i247424

33. Copeland R. A., Lombardo D., Giannaras J., & Decicco C. P. Estimating KI values for tight binding inhibitors from dose-reponse plots. *Bioorganic & Medicinal Chemistry letters*, **1995**, 5(17), 1947-1952. https:// doi.org/:10.1016/0960-894X(95)00330-V.

34. Copeland R. A., Lombardo D., Giannaras J., & Decicco C. P. Estimating KI values for tight binding inhibitors from dose-reponse plots. *Bioorganic & Medicinal Chemistry letters*, **1995**, 5(17), 1947-1952. https://doi.org/:10.1016/0960-894X(95)00330-V.

35. Li H., Sutter J., Hoffmann R., Pharmacophore Perception, Development and use in Drug Design, Güner O. F., Ed.; International University line : san Diego, CA, USA, **2000**; PP. 171-189.

36. Binda C., Li M., Hubalek F., Restelli N., Edmondson D. E., Mattevi A.. Insights into the mode of Inhibition of Human Mitochondrial Monoamine Oxidase B from high-Resolution Crystal Structures. *Proc. Natl. Acad. Sci. U.S.A.*, **2003**, 100, 9750-9755.

37. Binda C., Hubalek F., Li M., Herzig Y., Sterling J., Edmondson D. E., Mattevi A.. Crystal Structures of MAO B in Complex with Four Inhibitors of the N-Propargyl-aminoindan Class. *J. Med. Chem.*, **2004**, 47, 1767-1774.

38. William J.A., David R. B,. Steered Molecular Dynamics Simulations Reveal Important Mechanisms in Reversible Monoamine Oxidase B Inhibition *Biochemistry*, **2011**, 50, 6441-6454. https://doi.org/10.1021/bi200446w.

39 John, S.; Thangapandian, S.; Sakkiah, S.; Lee, K.W. Potent BACE-1 inhibitor design using pharmacophore modeling, *in silico* screening and molecular docking studies. *BMC Bioinform*. **2011**, 12, S28.

40. Available Chemicals Directory, version 95.1, MDL Information Systems, San Leandro, CA. **2003**. Available online: https://cds3.dl.ac.uk/cds/cds.html .

41. QikProp, version 3.7, release 14; X Schrödinger, LLC: New York, NY, **2014**

42 Jorgensen W. L., Duffy E. M. Prediction of drug solubility from Monte Carlo simulations. *Bioorg. Med. Chem. Let.***2000**, 10, 1155-1158.

43. Binda C., Newton-Vinson P., Hubálek F., Edmonson D. E. & Mattevi A. Structure of human monoamine oxidase B, a drug target for the treatement of neurological disorders. *Nat. Struc. Biol.*, **2001**, 9(1), 22-26. https://doi.org/:10.1038/nsb732.

44. Duffy, E. M., & Jorgensen, W. L. Prediction of Properties from Simulations: Free Energies of Solvation in Hexadecane, Octanol, and Water. *J. Am. Chem. Soc.*,**2000**, *122*(12), 2878-2888. https://doi:10.1021/ ja993663t.